Northumbria Research Link

ORIGINAL RESEARCH ARTICLE

The Depositional Record
Open Access
A journal of the International Association of Sedimentologists

IAS
WILEY

Fluvio-lacustrine sedimentation in the Agadir-Tissint Feija (Anti-Atlas, Morocco): A promising palaeoclimate archive for the last glacial cycle in northwest Africa

Alexis Nutz[1,2] iD | Ola Kwiecien[3] | Sebastian F. M. Breitenbach[3] | Yanjun Cai[4] |
Giovanna Della Porta[5] | Jan Danisch[1] | Lahcen Kabiri[6] | Stéphane Bodin[1]

[1]Department for Geoscience, Aarhus University, Aarhus, Denmark

[2]Centre Européen de Recherche et d'Enseignement des Géosciences de l'Environnement, Aix-Marseille Université, CNRS, IRD, Collège de France, INRA, Aix en Provence, France

[3]Ruhr-Universität Bochum, Geology, Mineralogy & Geophysics, Sediment and Isotope Geology, Bochum, Germany

[4]State Key Lab of Loess and Quaternary Geology, Institute of Earth Environment, Chinese Academy of Sciences, Xi'an, China

[5]Earth Sciences Department, Milan University, Milan, Italy

[6]Département de Géologie, Faculty of Science and Technology of Errachidia (FSTE), Université Moulay Ismail (UMI), Errachidia, Morocco

Correspondence
Alexis Nutz, Department for Geoscience, Aarhus University, Aarhus, Denmark.
Email: nutz@cerege.fr

Abstract

Mountainous depocentres are often the single available archives in intracontinental areas. As such, the investigation of their sedimentary dynamics is the only way to reconstruct palaeoenvironmental evolution in these peculiar regions. Here, the basin-scale sedimentary dynamics of the Agadir-Tissint Feija (i.e. feija is the local name for lowlands) are discussed together with new palaeoenvironmental information on the late Quaternary in the north-western Sahara margin. The succession consists of up to *ca* 40 m thick fluvio-lacustrine deposits subdivided into three depositional sequences (S1–S3) that were deposited between *ca* 75 ka and *ca* 10 ka. S1 and S2 reflect the evolution of a palaeolake intercalated by carbonate-rich palustrine to alluvial plain environments, while S3 shows the transition to an entirely clastic alluvial plain environment. The three sequences are genetically associated with three pulses of tufa buildups at the outlet of the depocentre. Each pulse of tufa buildup is attributed to wet conditions, while each interruption is associated with drier conditions. The wet–dry alternation at the origin of S1 fits with summer insolation fluctuation suggesting that precession parameters may have paced long-term climate variability in the area. Superimposed on wet–dry cycles, submillennial-scale (750–900 year) shorter-term lake fluctuations are identified in S1 and S2; their origins may be related to North Atlantic Oscillation mechanisms. Furthermore, the sudden increase in clastic sediment supply in S3 evidences a change in sediment production in the catchment area attributed to lower temperatures established during the last glacial period. Finally, this newly identified continental archive is unique at the northern Sahara margin; it enables reconstructions of the local and regional hydrological conditions during the last glacial cycle. Even if a more systematic investigation of palaeoclimate forcing is still necessary, the Agadir-Tissint Feija will potentially bring important information to understand past and anticipate future regional climate change.
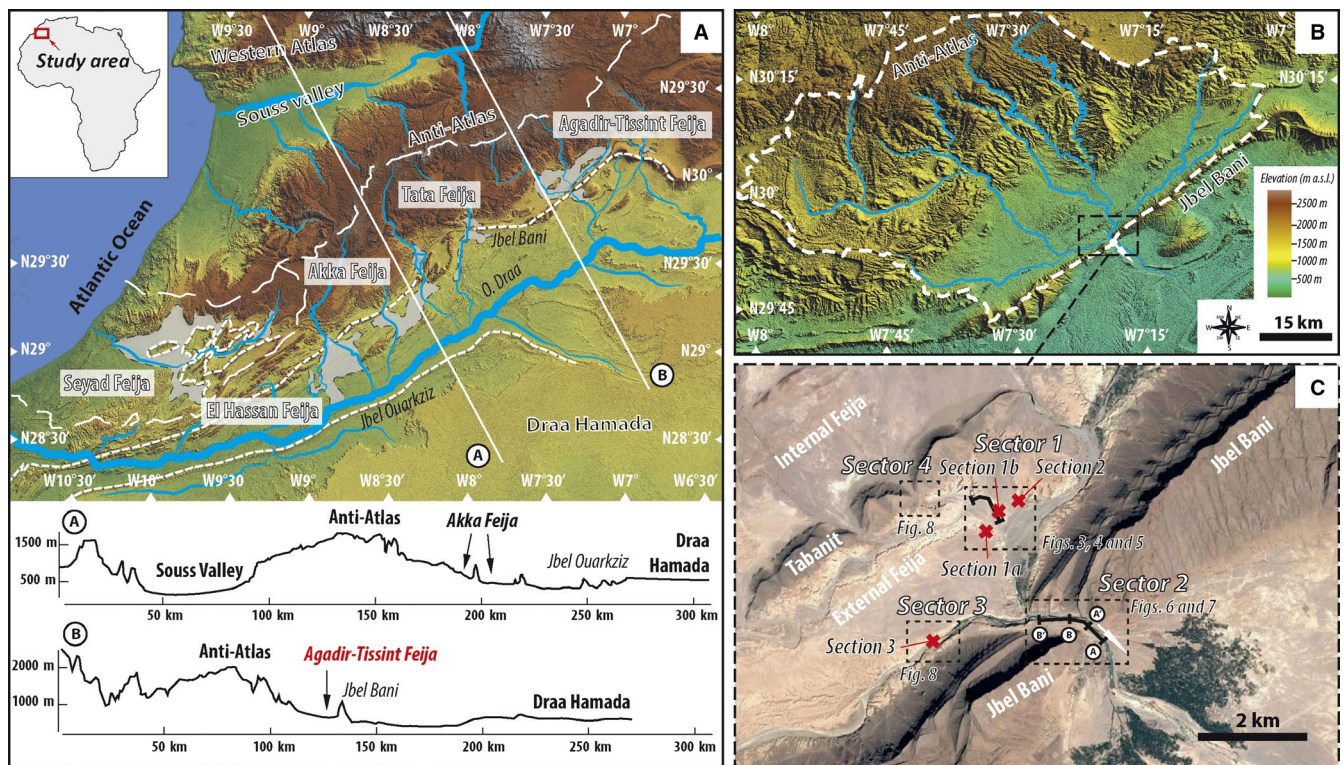
KEYWORDS
Anti-Atlas, foreland, Morocco, palaeolake, Pleistocene, tufa

---

1 | INTRODUCTION

Northwest Africa constitutes a transitional climatic zone influenced by Atlantic, Western Mediterranean and Saharan air masses (Kuhlmann, Meggers, Freudenthal, & Wefer, 2004; Tierney, Pausata, & deMenocal, 2017; Zielhofer et al., 2017). However, the lack of pre-Holocene continuous continental archives impedes long-term continental palaeoenvironmental reconstructions and limits the understanding of the interactions between these different air masses. Continental late Quaternary sedimentation in northwest Africa took place predominantly in mountainous domains in foreland depressions, which are rarely utilized at their full potential as archives of palaeoenvironmental changes. Active tectonic features delineate most of the investigated foreland depressions and this fact predisposes the scientific emphasis on the deconvolution of the tectonic and climate controls. Moreover, the deconvolution of the respective influence of tectonic and climate controls is mostly achieved through the examination of alluvial fan fluctuations in their overall size, grain size or the identification of aggradation–degradation cycles (e.g. Fang et al., 2016; Godard et al., 2014; Terrizzano et al., 2017); hence, concomitant depositional systems (i.e. alluvial plain or lacustrine) are frequently overlooked. This points to (a) the rarity of basin-scale sedimentological investigations of foreland depressions and (b) the difficulties in isolating the role of tectonic and climate forcing in such depocentres suggesting that they are complex archives for palaeoenvironmental reconstructions. At the same time, foreland depressions in tectonically stable areas, where sedimentation is mostly climate-controlled, remain less explored even though these largely overlooked sedimentary settings have great potential of recording environmental changes.

The here presented, new sedimentological data from Agadir-Tissint Feija (Anti-Atlas, Morocco), an exemplary foreland depression in a tectonically stable setting, address this paucity. Although several authors identified upper Quaternary deposits in the region (Andres, 1977; Dijon, 1976; Thorp, Glanville, Stokes, & Bailey, 2002; Weisrock, 2003), no detailed sedimentological characterization has been carried out; consequently the evolution of depositional systems remains unknown. Hereafter, building upon facies and sequence analyses, clay mineralogy and datings (U/Th), the Agadir-Tissint Feija sedimentary succession is investigated in detail. The successive depositional environments are described in different sectors of the depocentre. Then, sectors are correlated providing a basin-scale view of

FIGURE 1 Location maps. (a) Digital elevation model of south-western Morocco showing the Anti-Atlas and its surrounding areas. The five feijas identified in southern Morocco are indicated (modified after Thorp et al., 2002). Topographic profiles reveal that feijas constitute the first lowlands southward of the Anti-Atlas. (b) Digital elevation model of the Agadir-Tissint Feija catchment. The main rivers draining the area are represented as well as the catchment area of the Tissint depocentre. (c) Satellite image (Google Earth Pro, 2016) showing the investigated depocentre. Locations of sections and sectors presented in this study are given

the Agadir-Tissint Feija. Sedimentary motifs of (a) humidification/aridification cycles, (b) superposition of such cycles and (c) changes in sediment supply are described. The Agadir-Tissint Feija case study confirms and highlights the relevance of tectonically stable foreland depressions as valuable archives of Quaternary palaeoclimate, and reports, for the first time, the existence of a late Quaternary palaeolake at the north-western fringe of Sahara. Its level fluctuations reveal several episodes of greening during the last glacial cycle. Finally, although investigations of this peculiar system are at an early stage, they will probably provide important new insights on north-western African palaeoclimate.

2 | GEOLOGICAL BACKGROUND

The Anti-Atlas relief originates from the inversion of a thick (>10 km) latest Neoproterozoic to Palaeozoic succession. This inversion took place mostly during the Variscan orogeny (Burkhard, Caritg, Helg, Robert-Charrue, & Soulaimani, 2006; Michard, Hoepffner, Soulaimani, & Baidder, 2008) that formed a *ca* 140 km wide anticline currently reaching *ca* 2,000 m a.s.l. in its central portion (Figure 1a). This has led to the development of an organized drainage networks. Since that time, the southern flank of the Anti-Atlas is drained southwards by several rivers, now all tributaries to the Oued Draa, which constitutes the main fluvial system in southern Morocco (Figure 1a). Between the southern front of the Anti-Atlas and the escarpment of the Jbel Bani, these rivers leave narrow valleys and feed extensive 15–50 km wide lowlands locally called 'Feijas' (Figure 1a,b). These feijas originated from differential erosion of clay-dominated Middle Cambrian and Lower Ordovician rocks and more resistant sandstone-dominated and limestone-dominated Lower Cambrian and Upper Ordovician rocks (Michard, 1976). In places, a competent Middle Cambrian sandstone interval forms the Tabanit Ridge that separates internal and external feijas (Figure 1c, Michard et al., 2008). Five different feijas associated with five different rivers are recognized along the southern flank of the Anti-Atlas (Thorp et al., 2002; Figure 1a). They corresponded to important Late Quaternary depocentres (Andres, 1977; Dijon, 1976; Thorp et al., 2002; Weisrock, 2003) consisting of alternating fluvial and lacustrine sediments. Currently, the feijas are incised, indicating that sedimentation ceased, and sediments are now eroded and exported downstream.

The Agadir-Tissint Feija is *ca* 20 km long and *ca* 6 km wide, representing a *ca* 120 km^2 lowland connected to a catchment area >3,200 km^2 (Figure 1b). Northward, the catchment drains the southern flank of the Anti-Atlas with various lithologies exposed. Crystalline Proterozoic rocks (e.g. Gasquet, Ennih, Liégeois, Soulaimani, & Michard,

2008; Michard et al., 2008) overlain by Proterozoic volcano-sedimentary rocks, which are referred to as the Anti-Atlas and the Ouarzazate Supergroups (e.g. Thomas et al., 2004), occasionally crop out in 'boutonnières' (i.e. local name of klippe). Nevertheless, the dominant lithology in the catchment area consists of uppermost Neoproterozoic to lowermost Cambrian limestones of the Adoudounian and Lie de Vin Formations (e.g. Alvaro, Benziane, Thomas, & Walsh, 2014; Maloof et al., 2010). Southward, the catchment includes the northern flank of the Jbel Bani mainly composed of upper Ordovician shales and sandstones (Dietrich et al., 2018; Ghienne, Le Heron, Moreau, Denis, & Deynoux, 2007; Loi et al., 2010; Nutz, Ghienne, & Storch, 2013). In the Agadir-Tissint Feija, the more competent Tabanit Ridge separates internal and external feijas (Figure 1c, Michard et al., 2008). Downstream the external feija, a gorge crosses the Jbel Bani. This gorge constitutes the modern outlet of the system (Figure 1c).
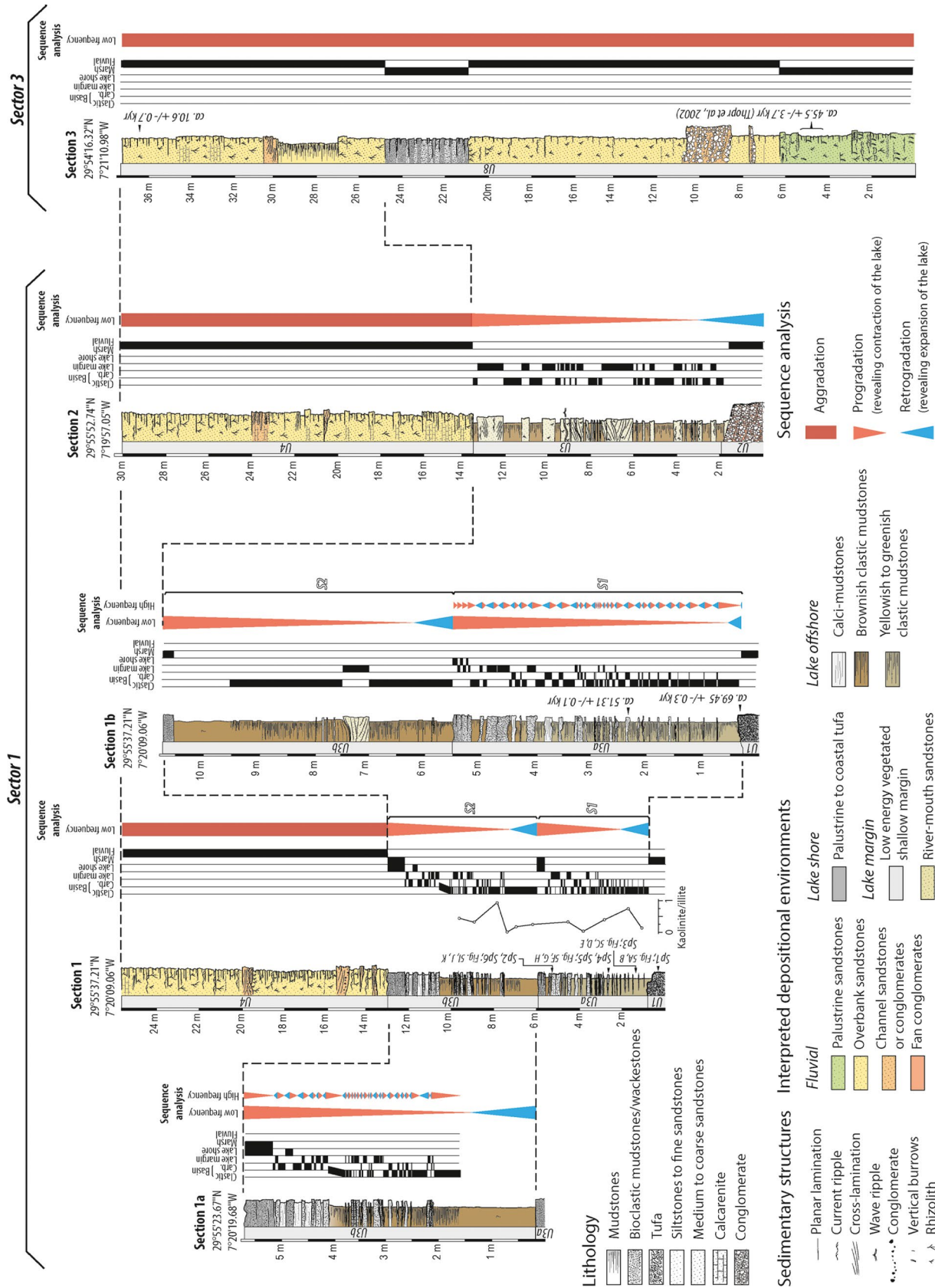
3 | METHODOLOGY

3.1 | Sedimentological and petrological analyses

Following initial survey based on satellite imagery (Landsat, SRTM1), three field surveys were conducted in October 2016, February 2017 and January 2018. Five sections (Figure 2) along river incisions were measured and multiple panoramas were analysed. Sedimentary facies (Table 1) have been interpreted based on macroscopic examinations from field surveys; lithology, grain size, sorting, bed thickness, sedimentary structures and palaeocurrents have been assessed based on conventional facies analysis. In addition, two samples (Sp1–Sp2) representing two different facies were described based on microscopic observations that have been made through petrographic analysis of 30 μm thin sections using a polarized light microscope Zeiss Axioskop and with a Zeiss Stemi SV6 both equipped with a Nikon digital camera. Lateral continuity and evolution of prominent stratigraphical surfaces were visually traced within the depocentre from the central portion to the different borders allowing basin-scale correlations. Subsequently, sequences were delineated in accordance with Catuneanu et al. (2009) considering a sequence as a full cycle of change in accommodation space, involving an increase followed by a decrease in the space available for sediments to fill.

3.2 | SEM imaging

Scanning electron microscopy analysis was performed on four samples (Sp3–Sp6) from sequence 1 (see Figure 2 for sample location). Gold-coated samples were analysed using a

FIGURE 2 Measured sections (see locations Figure 1c). Lithologies and sedimentary structures allowed the interpretation of eight depositional environments. Delineated sequences, basin-scale correlations and available ages are presented

Table 1   Lithofacies description and interpretation

Facies	Lithologies, texture, structures and bedding characteristics	Interpretation	Depositional environments
Mudstones			
Clastic mudstones (F1)	Yellow to light brown and dark brown; siliciclastics and detrital carbonates; fine silt to clay; dm-scale draping beds; massive to faintly laminated; occasional cm-scale erosional-based fining-up sequences; occasional dm-thick and m-scale wide lobate laminated beds	Suspension-fallout deposits; dominant detritic supply; occasional low-density turbidites; occasional bottom currents; below the limit of the subaqueous vegetation development	Offshore lake fed by active rivers (Potter, Maynard, & Pryor, 1980)
Calci-mudstones	White; euhedral to subhedral calcite crystals (microsparite with 5–20 μm crystal size); cm to dm-scale draping beds; laminated; microsparite coats moulds of filamentous organisms (10 μm), probably algae as *Oocardium*	Suspension-fallout deposits; calcite precipitation in supersaturated water; no detritic supply; below the limit of the subaqueous vegetation development	Offshore lake associated with inactive rivers (Bustillo et al., 2002)
Bioclastic mudstones to wackestones (F3)	White to beige; subhedral calcite crystals (microsparite with 5-20 μm crystal size); dm-scale to m-scale beds; massive; abundant moulds of plant stems and charophytes algae; rare gyrogonites; rare gastropodes	Suspension-fallout deposits; calcite precipitation in supersaturated water; low clastic content; above the limit of the subaqueous vegetation development	Shallow lake margin (Bustillo et al., 2002)
Tufa			
Phytoherm boundstones of stems (F4)	(a) Horizontal dm-scale long coated stems; mm-scale to cm-scale in diameter; carbonate coating made of rare clotted peloidal micrite followed by mm-scale crusts of fibrous calcite crystal fans	In situ coating of stems (probably of reed) by calcite precipitation due to freshwater supersaturation while flowing; growing upward; bended by flow	(a) Moderate-energy to high-energy fluvial area (Arenas-Abad et al., 2010)
	(b) Vertical dm-scale long coated stems; mm-scale to cm-scale in diameter; carbonate coating made of rare clotted peloidal micrite followed by mm-scale crusts of fibrous calcite crystal fans	In situ coating of stems (probably of reed) by calcite precipitation due to freshwater supersaturation while flowing; growing upward	(b) Palustrine; Lake shore (Arenas-Abad et al., 2010; Pedley, 1990)
	(c) Curtain of hanging dm-scale to m-scale long coated stems; mm-scale to cm-scale in diameter; covering topographic step; carbonate coating made of rare clotted peloidal micrite followed by mm-scale crusts of fibrous calcite crystal fans	In situ coating of stems (probably of reed) by calcite precipitation due to freshwater supersaturation while flowing; growing downward	(c) Cascade (Arenas-Abad et al., 2010)
Bryoherm boundstones of mosses (F5)	Dm-scale bushes of coated moss plants; empty interior cavities or filled by micrite	In situ coating of mosses by calcite precipitation due to freshwater supersaturation while flowing	Moderate-energy to high-energy active fluvial area; waterfalls (Arenas-Abad et al., 2010; Pedley, 1990)
Microbial boundstones (F6)	(a) Tabular; cm-scale horizontal or undulating layers; common fenestrae (primary irregular voids parallel to bedding)	Precipitation of calcite influenced by microbial mats and physico-chemical CO_2 degassing due to water flow; tabular and mound-shaped bioherms	(a) Fast-flowing fluvial area (Arenas-Abad et al., 2010)
	(b) Mound-shaped; dm-scale to m-scale bioherms; common fenestrae (primary irregular voids parallel to bedding)		(b) Calm fluvial area or lake shore (Arenas-Abad et al., 2010)

(Continues)

TABLE 1 (Continued)

Facies	Lithologies, texture, structures and bedding characteristics	Interpretation	Depositional environments
Intraclastic packstones (F7)	Dm-scale to m-scale tabular beds; mm-scale to cm-scale fragments of stems and microbial mats; occasional clastics and detrital carbonates; rare shell debris; dm-scale to m-scale through cross-laminations; occasional fining-upward intervals	Tractional deposition from dilute flow; lower flow regime conditions; occasional turbulent flows	High-energy fluvial area (Arenas-Abad et al., 2010)
Sandstones			
Lobate (F8)	Well-sorted medium sand; dm-scale to m-scale lobate beds; siliciclastics and detrital carbonates; prevailing planar laminations; frequent cm to dm through cross-laminations and occasional wave ripples; commonly interbedded by draping cm-scale to dm-scale mud beds	Tractional deposition from dilute flow; lower flow regime conditions; migrating 2D dunes or bars in places reworked by oscillatory currents; draped by mud settling during episodes of flow interruptions	River mouth bar in shallow lake margin (Nutz et al., 2015; Schomacker et al., 2010)
Tabular (F9)	Well-sorted fine and medium sand; cm-scale to dm-scale beds; siliciclastics and detritic carbonates; cm-scale current ripples and occasional climbing ripples in medium sand; planar to draping laminations in fine sand; frequent roots; common vertical burrows	Traction deposition from dilute flow; lower flow regime conditions; alternations of sand sheets and low-energy fine sedimentation in shallow ponds; repeated bioturbation by plants and fauna	Overbank deposits in alluvial plain (Miall, 2014)
Lenticular (F10)	Moderately sorted sand; cm-scale to m-scale beds; siliciclastics and detrital carbonates; planar and through cross-laminations; occasional pebbles	Tractional deposition from dilute flow; lower flow regime conditions; bedoad transport by dunes and bars	Fluvial channel or river mouth channel in shallow lake margin
Conglomerates			
Lenticular (F11)	Matrix-supported conglomerate; siliciclastics and detrital carbonates; well-rounded to flat cm-scale clasts; frequent dm cross-laminations; occasional dm-scale beds of massive sand to gravel	Tractional deposition from dilute flow; lower flow regime conditions; bedload transport associated with occasional debris flows	Fluvial channel (Miall, 2014)

LEO/Zeiss Gemini 1530 operating with an acceleration voltage of 20 kV. Identification of the chemical composition of the minerals was achieved by use of energy-dispersive X-ray spectroscopy (EDX) system and the AZTec software package from OXFORD Instruments.

3.3 | Datings

Dating data set includes eight ages (Table 2), two optically stimulated luminescence (OSL) ages from a previous study (Thorp et al., 2002) and six from this study. Six U/Th ages were measured on carbonate rocks at the Institute of Global Environmental Change, Xi'an Jiaotong University. Samples of 60–80 mg of carbonate powder drilled from the tufa were dissolved for separation of uranium and thorium. The chemical U and Th separation procedure is similar to that described by Edwards, Chen, Ku, and Wasserburg

(1987). The measurements were made on the Thermo-Scientific Neptune MC-ICP-MS equipped with tan Aridus II desolvating nebulizer. The data were acquired using the peak-jumping acquisition protocol on the SEM, similar to those described in Cheng et al. (2013). Here we use the bulk earth value with large error of 50%, i.e. $4.4 \pm 2.2 \times 10^{-6}$, for the initial thorium correction. The measured isotope ratios of uranium and thorium, and the calculated ages are listed in Table 2.

3.4 | XRD analysis

A total of 11 samples collected in the central portion of the depocentre (sector 1) were analysed using X-ray diffraction (XRD) at the Department of Geoscience, Aarhus University (Denmark). XRD instrument is a PANalytical X'Pert Pro MPD. Analyses were performed on oriented mounts of

TABLE 2 Compilation of available ages in the Agadir-Tissint Feija

	Sample number	^{238}U (ppb)	^{232}Th (ppt)	^{230}Th/^{232}Th (atomic ×10^{-6})	d^{234}U^a (measured)	^{230}Th/^{238}U (activity)	^{230}Th Age (year) (uncorrected)	^{230}Th Age (year) (corrected)	d^{234}U$_{initial}$^{b}	^{230}Th Age (yr BP)^c (corrected)	
U/Th	Ti_S10_007	3,473	30.2997	59	1,808.5 ± 2.4	0.3147	12,804 ± 25	11,917 ± 629	1,870 ± 4	11,850 ± 659	This study
	Ti_S1_014	14,475	79,572	3,205	1,720.7 ± 2.9	1.0685	51,434 ± 147	41,381 ± 151	1,989 ± 3	51,314 ± 151	
	W53-U2	41,64.3 ± 10.1	22,828 ± 459	3,720 ± 75	1,483 ± 2.8	1.2366	69,578 ± 260	69,521 ± 263	1,805 ± 4	6,9454 ± 263	
	Ti_S4_005	41,05.6	56,441	1,571	1,615.0 ± 2.2	1.3100	69,953 ± 146	69,818 ± 174	1,967 ± 3	69,751 ± 174	
	W53-U1	42,22.2 ± 10.3	74,005 ± 1486	1,196 ± 24	1,469.8 ± 2.8	1.2714	72,691 ± 283	7,2509 ± 310	1,803 ± 4	72,442 ± 310	
	W53-U3	3,868.6 ± 10.2	91,017 ± 1,829	916 ± 18	1,475.4 ± 3.00	1.31	75,411 ± 308	75,167 ± 352	1,824 ± 4	75,100 ± 352	
	Sample number	Equivalent dose (Gy)	K (%)	Th (ppm)	U (ppm)	Depth (m)	Cosmic (Gy/ka)	Moisture	Dose rate (Gy/ka)	OSL age	
OSL	Sample 1	40.6 ± 2.1	2.32 ± 0.04	7.26 ± 0.10	3.74 ± 0.05	<1	0.20 ± 0.02	0.01 ± 0.03	3.82 ± 0.15	10.6 ± 0.7	Thorp et al. (2002)
	Sample 3	72.1 ± 4.3	0.52 ± 0.02	2.44 ± 0.03	7.75 ± 0.14	25	0.03 ± 0.01	0.50 ± 0.07	1.60 ± 0.09	45.0 ± 3.7	

decarbonated clay-sized particles (<2 μm). For each sample, three XRD runs were analysed after air-drying, ethylene–glycol solvation and heating at 500°C for 1 hr. Proportions of the different main clay phases are reconstructed for each sample based on diffractogram analyses. Ratios of kaolinite and chlorite were particularly regarded in each sample aiming at reconstructing evolution of the weathering intensity in the catchment.

4 | RESULTS

4.1 | Sedimentological and stratigraphical analyses

Four sectors (Figure 1c) have been distinguished in the depocentre, (a) central portion, (b) the outlet, (c) south-western and (d) north-eastern margins. For each sector, allostratigraphic sedimentary units (U) are identified. These allostratigraphic units delineate sediment accumulations with uniform lithologies regarding a particular sector, although potentially with lateral lithology, facies or facies association changes from sector to sector, and bounded by unconformities or their correlative conformities. Units are described and interpreted through a facies-based nomenclature (F1–F11, Table 1). Description results from macroscopic and microscopic examinations that constitute the basis for interpretation of depositional environments in all sectors. The temporal succession of different depositional environments allows delineating sediment packages that reflect the evolution of accommodation space and transgressive–regressive (T–R) cycles through time. Finally, the four sectors are correlated within two transects which represent both the basin-scale architecture and depositional environments.

4.1.1 | Facies description and interpretation

Eleven sedimentary facies are identified in the Agadir-Tissint Feija and details of their interpretation are provided in Table 1. Facies are subdivided into three groups. The first group includes mudstones (i.e. siliciclastic and/or carbonate grains inferior to 63 μm) to wackestones (F1–F3) originated from dominant suspension-fallout processes and/or in situ precipitation of carbonate attributed to a sedimentation in low-energy subaqueous lacustrine environments (cf. Potter et al., 1980). F1 and F2 mostly differ in the nature of their major components. F1 is a clastic mudstone, while F2 is a calci-mudstone (sensu Wright, 1992). F3 is a bioclastic calci-mudstone to wackestone with bivalves and charophytes indicative of shallower depositional environments where subaqueous vegetation was able to develop. In the following, the lower boundary of vegetation development in the subaqueous domain is considered to separate offshore lake and

lake margin depositional environments. The second group consists of carbonate deposits (F4–F7) in km-scale carbonate beds. These sedimentary facies represent carbonates precipitated in freshwater under subaerial and ambient temperature conditions and as such they are interpreted as carbonate tufa (Ford & Pedley, 1996; Pedley, 1990). Consequently, F4–F7 facies are classified using the terminology proposed by Arenas-Abad, Vazquez-Urbez, Pardo-Tirapu, and Sancho-Marcéen (2010) which describes tufa in either lake shore or fluvial domains. The third type of sedimentary facies includes sandstones and conglomerates (F8–F11) reflecting deposition from mostly dilute flows attributed to the activity of a river system (Miall, 2014; Nutz et al., 2015; Schomacker, Kjemperud, Nystuen, & Jahren, 2010).

All these sedimentary facies (Table 1) point to the existence of ancient lacustrine-to-fluvial sedimentary systems and document depositional environments such as offshore lake, lake margin, lake shore, fluvial cascade, alluvial plain and alluvial fan.
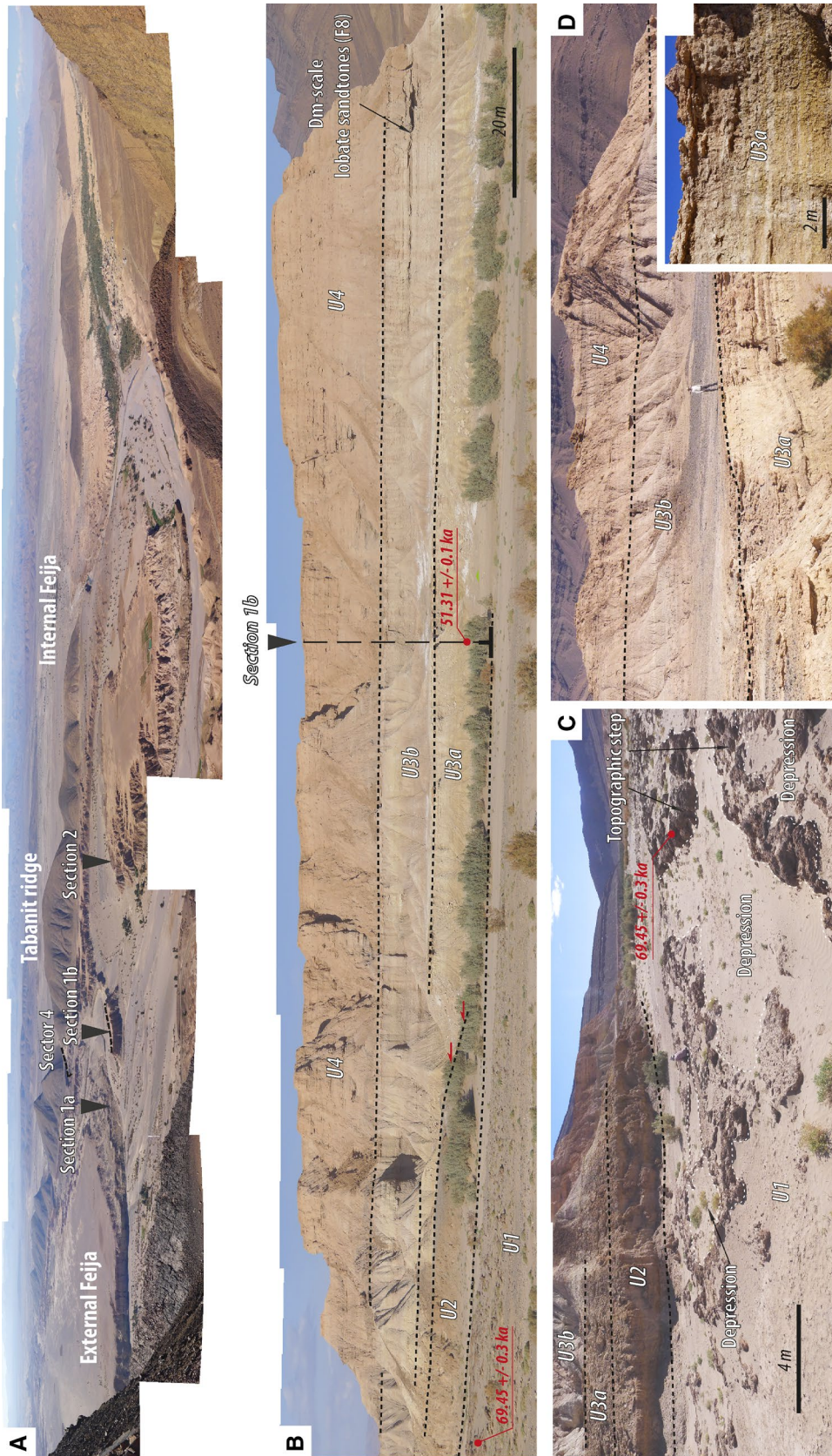
4.1.2 | Sector 1: The central portion

Depositional environments

In the central part of the Agadir-Tissint Feija (Figure 1c), the current river incision exposes a 27 m thick succession along several hills (Figures 2 and 3a). Three sections 1a, 1b and 2 were logged in this sector (Figures 1 and 2) and the exposed succession is divided into four units (U1–U4; Figure 3b).
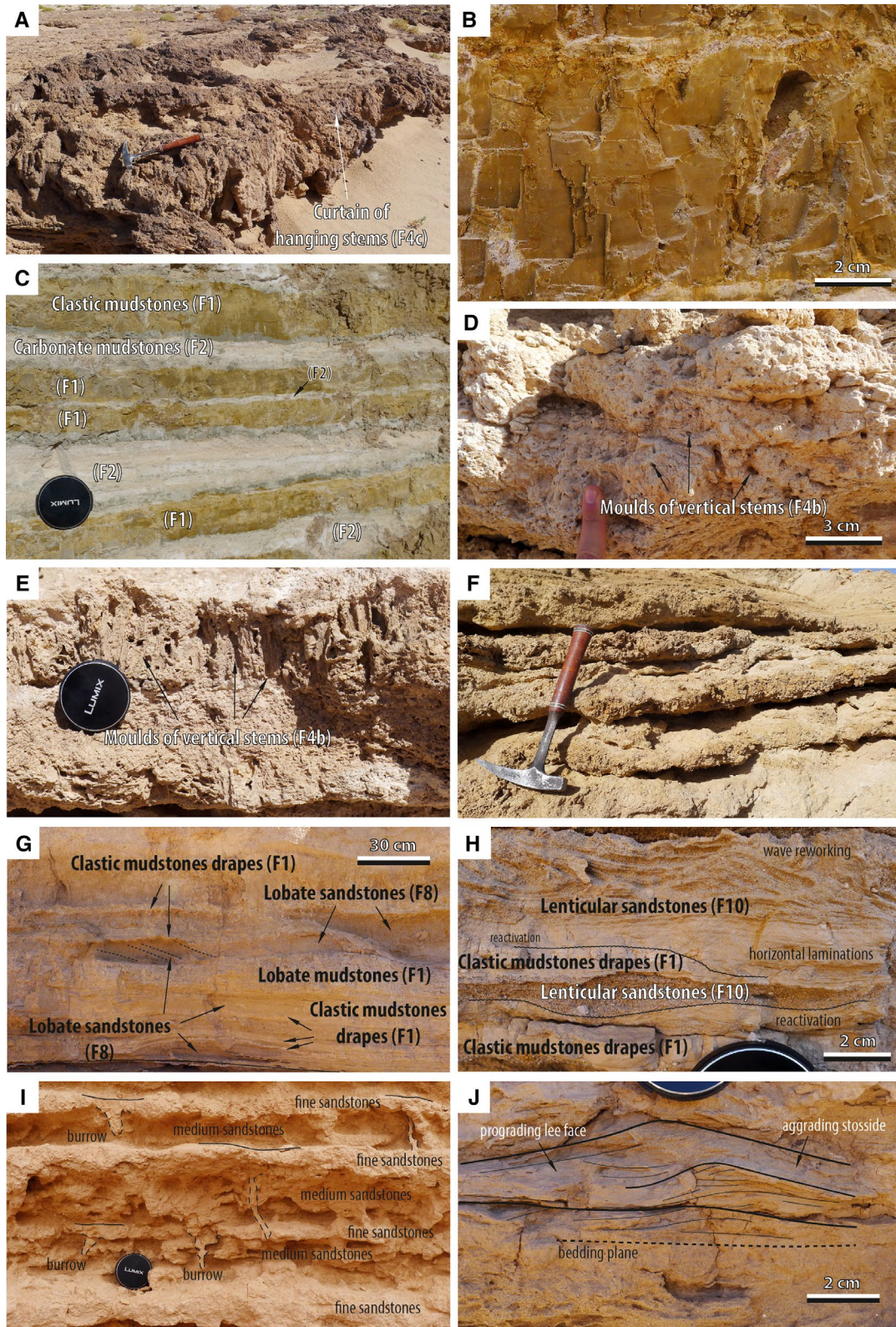
U1 is a m-scale carbonate-rich interval of which the lower boundary is not exposed. U1 is composed of dm-scale to m-scale phytoherm boundstones of stems (F4). In places, phytoherm boundstones of vertical stems (F4a) encircle depressions located at different elevations, connected by steps (Figures 3c and 4a) made of curtains of hanging stems (F4c) (Figure 5a,b). The lateral juxtaposition of depressions and steps form an uneven upper surface. Above, the unit U2 is a 2 m thick conglomerate (Figure 2, section 2) that conformably overlies U1. U2 pinches out southward and disappears near section 1b (Figures 2 and 3b) forming a km-scale lobe. In places, 100 m long, low-angle (<5°) oblique southward dipping master beds are identified. U2 includes lenticular conglomerate (F11), occasionally associated with lenticular sandstones (F10). The overlying unit U3 is a *ca* 11–12 m thick mud-dominated sediment package that seals U1 and onlaps U2 (Figure 3b). In section 1b, U3 is divided into subunits U3a and U3b (Figures 2 and 3b–d). U3a comprises a 5 m thick interval including cm-scale to dm-scale beds of yellowish to greenish clastic mudstones (F1) (Figures 3e, 4b, and 5c,d,e) alternating with whitish calci-mudstones (F2) (Figures 3e, 4c, and 5f,g,h). This interval is topped by a *ca* 1 m thick interval made of bioclastic calci-mudstones to wackestones (F3) (Figures 3e, 4d, and 5i,j,k) that grades laterally to phytoherm boundstones of vertical stems (F4b) (Figure 4e,f). Above,

U3b consists of a *ca* 6 m thick interval of alternating brownish clastic (F1) and calci-mudstones (F2). In the middle, a dm-scale bed made of juxtaposed lobate sandstones (F8) is observed (Figures 3b and 4g,h). U3b is topped by a 1.5 m thick interval of alternating dm-scale beds of bioclastic calci-mudstones (F3) and dm-scale beds of phytoherm boundstones of vertical stems (F4b). In section 2, U3 consists of a heterolitic interval made of clastic mudstones (F1) recurrently interbedded by dm-scale lobate sandstones (F8) and occasionally by dm-scale lenticular sandstones (F10) (Figures 2 and 4g,h) with abundant rhizoliths. Finally, U4 is an 11–16 m thick sandstone-dominated unit showing similar facies in both sections 1b and 2. Tabular sandstones (F9) prevail generally in cm-scale to dm-scale beds (Figure 4i,j) although at two particular levels, 0.5–1 m thick and 10–100 m wide lenticular sandstones (F10) and conglomerates (F11) occur.
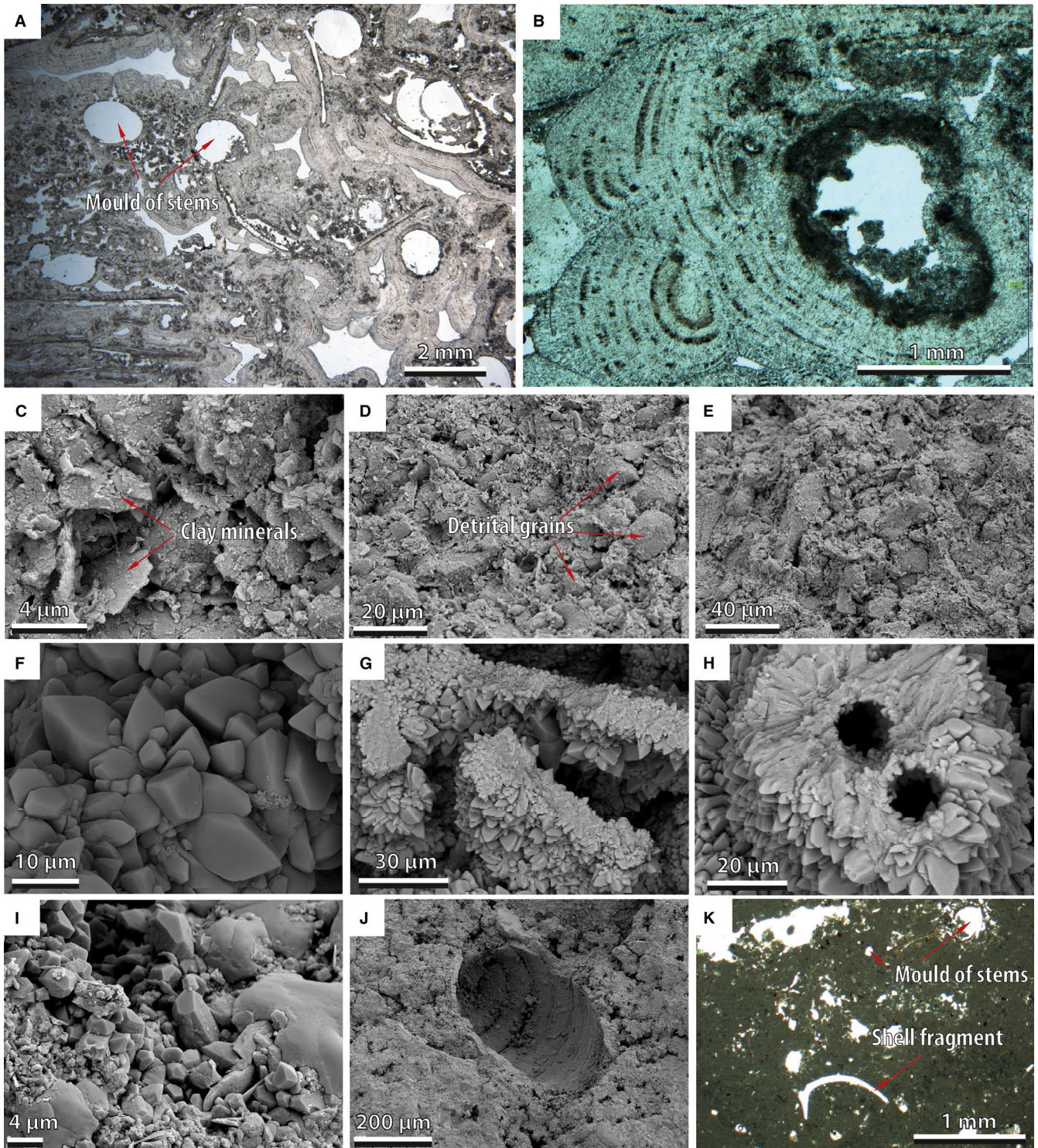
Depressions in U1, encircled by boundstones of vertical stems and connected by successive steps, reflect successive pools and cascades where hygrophilous plants were abundant (Figure 3c). Curtains of hanging stems characterizing topographic steps testify water flow from pool to pool. U1 is interpreted as a stepped fluvial tufa deposits in a low-energy alluvial plain environment (e.g. Arenas-Abad et al., 2010). Above, the combination of a lobate form and low-angle master beds dipping southward indicates that U2 is a large-scale depositional fan (Mather, Stokes, & Whitfield, 2017; Van Dijk, Postma, & Kleinhans, 2009), whose location in the central part of the lowlands, far from surrounding reliefs, allows attributing it to a terminal fan. Orientation of the wedge suggests that rivers came from the North/Northwest and led to southward progradation. U3 is dominated in section 1 by mud-sized sediment suggesting low-energy subaqueous settling through fallout. The lack of evidence for subaerial exposure indicates a perennial subaqueous domain while the absence of rhizoliths indicates a palaeo-depth of sedimentation below the limit of the vegetation development. In this study, this limits the offshore domain and thus U3 is referred to as offshore lacustrine deposits. Clastic mudstones reveal lacustrine periods during which rivers were feeding the lake and calcium supersaturation was prevented. On the other hand, calci-mudstones reflect periods during which rivers were inactive and the lake was supersaturated allowing carbonate precipitation (Arribas, Bustillo, & Tsige, 2003; Bustillo, Arribas, & Bustillo, 2002). Very limited clastic input and coeval supersaturation of the lake suggest a reduced precipitation and runoff into the lake, and increased evaporation. Calci-mudstones evidence periods of increased aridity with higher evaporation/precipitation (E/P) ratio that led to shallowing of the lake. Offshore lacustrine mudstones are separated by shallow lake margin sediments laterally associated with palustrine to fluvial tufa deposits (i.e. top of U3a and top of U3b). These deposits attest a marshy depositional environment with relative occasional ponds between emerged and vegetated areas. The dm thick

FIGURE 3 Sedimentary architectures in the central portion of the depocentre (sector 1, see location in Figure 1c). (a) Panorama showing Quaternary deposits incised by current rivers in the external feija, separated from the internal feija by the Tabanit Ridge. (b) Stratigraphic relationships between U1, U2, U3 and U4. (c) Close-up view of the top surface of U1 characterized by successive depressions and steps made of tufa deposits. (d) Stratigraphic relationships between U3 and U4. Note the remarkable surface between U3a and U3b. (e) Alternations of clastic (F1) and carbonate (F2) muds in U3a. At the top, bioclastic mudstones (F3) grading laterally to vertical phytoherm boundstones of stems (F4b) form a 0.5 m thick interval corresponding to the boundary surface between U3a and U3b

FIGURE 4 Macroscopic facies in the central portion of the depocentre (sector 1). (a) Curtain of hanging stems (F4c) forming steps at the top of U1. (b) Clastic mudstones (F1) in the lower part of U3a. (c) Alternations of clastic (F1) and calci-mudstones (F2) in the middle part of U3a. (d) Bioclastic mudstones (F3) at the top of U3a. (E and F) Moulds of vertical stems (F4b) in phytoherm boundstones constituting the uppermost part of U3a. (g) and (h) Alternations of clastic mudstones (F1) and lobate sandstones (F8) deposited in a river mouth environment. In places, reworking by waves is observed. (i) Alternations of cm-scale medium and fine sandstones in tabular sandstones (F9) interpreted as overbank deposits in floodplain environment. (j) Climbing ripples in tabular sandstones (F9)

FIGURE 5 Microscopic facies in the central portion of the depocentre (sector 1). (a, b and k) are thin-section pictures under plain polarized light. (c–j) are SEM pictures. (a) Boundstones of carbonate coated plant stems, probably reeds in U1. (b) Clotted peloidal micrite surrounding a mould of a stem followed by fibrous calcite crystal fans with undulose extinction coating the stem moulds with mm-thick crusts. (c) Close-up of view clay minerals in clastic mudstones. (d and e) Clay minerals and detrital grains in clastic mudstones (F1). (f) Euhedral to subhedral calcite crystals (5–20 µm in size) in calci-mudstones (F2). (g) Euhedral to subhedral calcite crystals (1–8 µm in size) in calci-mudstones (F2) probably precipitated around a filamentous-shaped organic substrate. (h) Euhedral bladed calcite crystals (20 µm long) departing radially from a hollow tube with a diameter of nearly 10 µm that might represent the mould of the filamentous alga *Oocardium* as observed in present-day freshwater tufa (cf. Gradziński, 2010; Rott, Hotzy, Cantonati, & Sanders, 2012). (i) Subhedral calcite crystals in bioclastic mudstones (F3). (j) Gyrogonite in bioclastic mudstones (F3) revealing the presence of charophytes. (k) Texture of bioclastic mudstones (F3). Structureless micrite with peloids, fragments of shells, stem of charophytes and mouldic and vuggy porosity

sandstone intercalated in the middle of U3b represents a river mouth bar deposited either during short-term lake shallowing or via more frequent and/or intensified flood events. In Section 2, alternating clastic mudstones (F1) and lobate sandstones (F8) are linked to the deposition of river mouth bars during river flood events recurrently draped by background settling of mud during low fluvial activity. These express a river-dominated lake margin. Abundance of rhizoliths suggests recurrent emersion episodes and high-frequency, low-amplitude lake-level fluctuations. Finally, U4 is dominated by overbank deposits, occasionally associated with fluvial channels in an alluvial plain environment. U4 marks the interruption of lacustrine conditions in the central portion of the depocentre and the transition to subaerial sedimentation.

Insights from clay mineralogy

The proportion of kaolinite and chlorite was measured in 11 samples to estimate the evolution of weathering intensity in the catchment. The kaolinite/illite ratio (K/I) is a robust proxy for weathering intensity as kaolinite is typically formed in soils developed from intense chemical weathering in warm and humid climates, whereas illite is derived from physical erosion of bedrock or formed by moderate chemical weathering of feldspar and micas (Chamley, 1989). Consequently, enhanced chemical weathering during warmer and wetter conditions led to further degradation of illite to kaolinite and a higher K/I ratio.

In the Agadir-Tissint Feija, the measured K/I ratios range from 0 to 0.4, indicating moderate chemical weathering during most of the U3 deposition. However, two samples in U3a and U3b, respectively, show very high K/I ratios around *ca* 0.7 and 0.9. These samples represent an abrupt intensification of chemical weathering during warmer and wetter episodes.

Sequence analysis and significance

Vertical stacking patterns are particularly well-preserved in the central portion of the depocentre allowing the delineation of two periodicities. The superposition from base to top of the low-energy fluvial tufa deposits (U1), the lacustrine offshore sediments (U3a) and the palustrine deposits (top of U3a) reveals a first lacustrine transgression followed by a lacustrine regression. This marks a complete transgressive–regressive (T–R) cycle referred to as S1 (Figure 2). Above the palustrine deposits (top of U3a), the overlying lacustrine deposits (U3b) grade upward to palustrine deposits and characterize a second T–R cycle, referred to as S2 (Figure 2). In both S1 and S2, the deposition of offshore lake facies above fluvial to palustrine deposits gives evidences of a rapid flooding of the depocentre. The maximum flooding interval is characterized by a relatively thick package dominated by clastic mudstones. Above, intervals of calci-mudstones progressively prevail, marking frequent and repeated episodes of lake shallowing. Finally, this progressive shallowing-upward succession ends with palustrine to fluvial tufa facies,

corresponding to the uppermost part of each sequence and marking an emersion interval. Clay mineralogy reveals that warmer and wetter conditions coincided with the maximum flooding interval in S1 and slightly later than to the maximum flooding interval in S2. This highlights that the two lacustrine sequences are tightly coupled to climatic fluctuations (wet–dry periods). Furthermore, shorter-term changes in depositional environments are superimposed on S1 and S2. Alternations of clastic and calci-mudstones and of clastic and bioclastic calci-mudstones reflect repeated changes between deep and shallower offshore lacustrine conditions or between offshore and lake margin environments. Both reveal shorter-term lake-level falls and lowstands due to increased E/P ratio during the overall longer-term lacustrine sequences S1 and S2. In total, 33 shorter-term lake-level falls are identified in S1, while 26 are recognized in S2 indicating climate instability that led to frequent moisture budget changes.

The development of lacustrine conditions in both S1 and S2 indicates that the rate at which accommodation space was created was higher than the sedimentation rate suggesting low to moderate sediment supply. Overlying these lacustrine sequences, the fluvial deposits of U4 show an aggrading pattern. This aggradation might represent either the upper part of S2 traducing an overall aggrading-prograding pattern or a third sequence associated with a new coeval cycle of accommodation space creation. In any case, the replacement of lacustrine conditions by fluvial sedimentation indicates that sediment supply exceeded accommodation space creation during the final stage of infill of the Agadir-Tissint Feija.

4.1.3 | Sector 2: The outlet

Depositional environments

Sector 2 corresponds to the Tissint gorge (Figure 1c) where modern river incision exposes a 12–20 m thick late Quaternary succession which comprises extensive and continuous tabular carbonate rocks. Although the vertical escarpments prevented detailed and systematic logging of the succession, the identification of unconformities that bounding sediment packages allowed the identification of three units referred to as U5, U6 and U7 (Figures 6a and 7a).

U5 is a *ca* 5 m thick carbonate succession. From base to top, facies consist of intraclastic packstones (F7), occasionally associated with lenticular sandstones (F10). Upward, intraclastic packstones and lenticular sandstones are not present anymore and sedimentation is dominated by microbial boundstones (F6). Microbial boundstones start with tabular microbial boundstones (F6a) forming planar beds (Figure 6b). Progressively, mound-shaped microbial boundstones (F6b) are intercalated with tabular microbial boundstones reaching m-scale wide and dm-scale high bioherms (Figure 6d,e). In the uppermost part, mound-shaped microbial boundstones prevail and reach tens of metres in width and up to 1 m in

height, forming an uneven surface at the top of U5. Above, U6 is a *ca* 4 m thick carbonate succession displaying a similar organization to U5. In the lowermost part, occasional intraclastic packstones are intercalated with tabular microbial boundstones that onlap the mound-shaped bioherms constituting the top surface of U5 (Figure 6a). Upward, similar to U5, tabular microbial boundstones (F6a) are progressively replaced by dm-scale mound-shaped bioherms grading upward to m-scale mound-shaped microbial boundstones (F6b). The overlying U7 is a *ca* 5 m thick carbonate succession that onlaps and seals the underlying top surface of U2 (Figure 6a). U7 is dominated by phytoherm boundstones of stems (F4) and bryoherm boundstones of mosses (F5; Figure 6a,f,g). In U7, cm-scale to dm-scale conglomerate lenses are common (F11) while microbial bioherms are rare. The top surface displays 2–3 m topographic steps (Figure 7), oriented downstream, and made of phytoherm boundstones of hanging stems (F4c) connecting flat areas made of phytoherm boundstones of vertical (F4a) and horizontal stems (F4b) and bryoherm boundstones of mosses (F5).

The extensive and continuous tabular pattern of carbonate rocks in sector 2 reveals a deposition from freshwater at ambient temperature conditions rather than from spring resurgence, which are more associated with mound geometries (e.g. Della Porta, 2015; Della Porta, Capezzuoli, & De Bernardo, 2017). These carbonate rocks meet the definition of tufa (Ford & Pedley, 1996; Pedley, 1990). Intraclastic packstones, lenticular sandstones and tabular microbial boundstones reveal moderate-energy to high-energy flows in a fluvial tufa environment (Arenas-Abad et al., 2010; Auqué et al., 2014; Pedley, 1990). Mound-shaped bioherms suggest relatively low-energy flow in calm fluvial areas or along lake shore (Arenas-Abad et al., 2010; Della Porta, 2015). Thus, both U5 and U6 display a vertical transition from moderate to high-energy fluvial tufa environments to lower-energy fluvial tufa or lake shore environments. This reflects the progressive transition in both U5 and U6 from fast-flowing water to slow-flowing to standing water; this evolution is considered to express a pulse of a tufa dam emplacement. The onset of the pulse is associated with the deposition of high-energy fluvial tufa. However, the deposition of fluvial tufa in sector 2 led to an aggradation that increasingly blocked and isolated water upstream, resulting in the development of a pond and then a lake. With pond extension, upstream flow was progressively impeded, and flow in the gorge reduced. With increasing lake surface, rivers did not reach the gorge any longer and waters flowing in the gorge had low-energy, resulting only

from the overflowing of the newly created dam. Finally, steps in U7 represent cascades, while phytoherm boundstones of horizontal stems and bryoherm boundstones of mosses reflect a return to recurrent moderate to high-energy flows. Continuous high-energy flow evidences a perennial fluvial tufa at the origin of a third pulse of tufa aggradation in sector 2. U7 is interpreted as a stepped fluvial tufa deposit (Arenas-Abad et al., 2010; Vazquez-Urbez, Arenas, & Pardo, 2012).

Sequence analysis and significance

Field observations reveal that some unit boundaries in sector 2 coincide with sector 1 unit boundaries (Figure 7). U5 and U6 grade laterally to the lacustrine deposits of U3a and U3b, while U7 passes laterally to U4. U5 and U6 coincide with S1 and S2, respectively, revealing that the two successive episodes of dam formation in the Tissint gorge produced the two successive lacustrine intervals in the central portion of the depocentre. The differentiation of U7 in sector 2 traduces a third pulse of tufa aggradation in the form of a stepped fluvial tufa. This third pulse of tufa construction reveals a third pulse of accommodation creation that defines a third sequence. U7 and U4 delineate a third sequence referred to as S3. S3 differs from S1 and S2 in that clastic sediment supply exceeded the creation of accommodation space. The newly created accommodation space was simultaneously filled by fluvial sediments of U4.
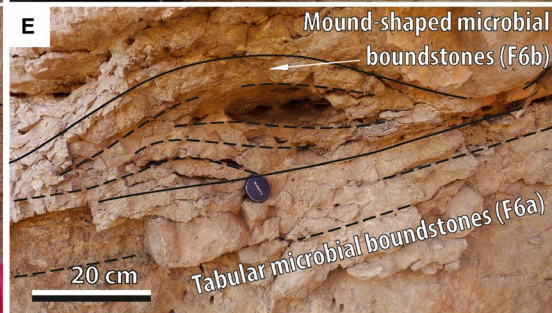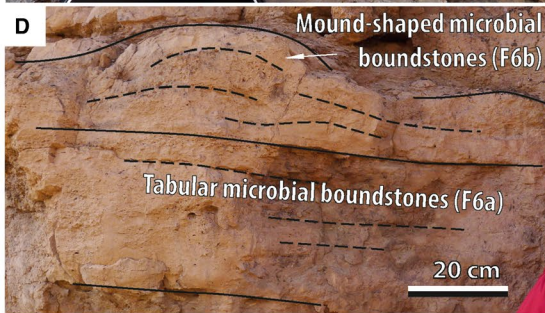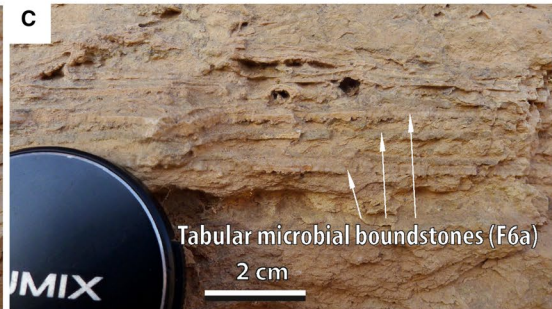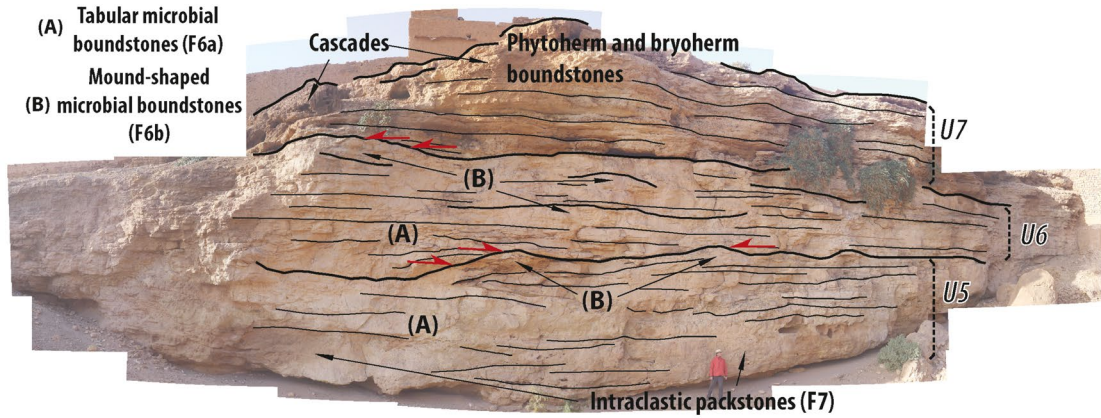
Summarizing, the Tissint Gorge deposits reveal three pulses of tufa constructions during the late Quaternary. These repeatedly created accommodation space in the depocentre at the origin of the three long-term sequences; the first two sequences were dominated by lacustrine sedimentation, while the last one was characterized by fluvial sedimentation in the central portion of the depocentre.

4.1.4 | Sectors 3: The south-western margin

Depositional environments

Sector 3 is located in the south-western part of the depocentre (Figure 1c) near the area studied by Thorp et al. (2002). It consists of a *ca* 37 m thick sandstone unit referred to as U8 (Figures 2 and 8a). U8 includes tabular sandstones (F9) intercalated with occasional intervals of lenticular sandstones (F10), lenticular conglomerates (F11), as well as a prominent carbonate-rich interval made of bioclastic calcimudstones to wackestones (F3) and phytoherm and bryoherm boundstones (F4 and F5). The unit starts with a *ca* 6 m thick coarse sandstone package (Figure 8b) composed of

FIGURE 6 Sedimentary architectures of the tufa dam in the Tissint gorge (sector 2, see location Figure 1c). (a) Panorama and interpreted panorama of the carbonate succession exposed in the Tissint gorge. Three units are identified. (b and c) Tabular microbial boundstones (F6a) forming the prevailing deposits in the lower part of U5 and U6. (d and e) Mound-shaped microbial boundstones (F6b) constituting the prevailing deposits in upper part of U5 and U6. (f) Bryoherm boundstones of mosses in U7. (g) Phytoherm boundstones of hanging stems (F4b and F4c, respectively) in U7

A

South (downstream)

North (upstream)

2 m

(A) Tabular microbial boundstones (F6a)

(B) Mound-shaped microbial boundstones (F6b)

Cascades

Phytoherm and bryoherm boundstones

U7

(B)

(A)

U6

(B)

U5

(A)

Intraclastic packstones (F7)

B Tabular microbial boundstones (F6a)

fenestrae

2 cm

C Tabular microbial boundstones (F6a)

2 cm

D Mound-shaped microbial boundstones (F6b)

Tabular microbial boundstones (F6a)

20 cm

E Mound-shaped microbial boundstones (F6b)

Tabular microbial boundstones (F6a)

20 cm

F Bryoherm boundstones of mosses (F5)

4 cm

G Curtain of hanging stems (F4c)

FIGURE 7 Panorama showing the lateral correlations between sector 2 in the Tissint gorge and sector 1 in the central portion of the depocentre. U5, U6 and U7 grade laterally to U3a, U3b and U4 revealing three basin-scale sequences referred to as S1, S2 and S3 (see Figure 1c for location of A, A′, B and B′)

dm-scale beds of tabular sandstones (F9) abundantly bioturbated by cm-scale branching burrows (Figure 8c). In places, it includes rounded depressions, 10 cm in diameter and 5 cm deep, encircled by a cm-high ridge (Figure 8d); these structures are interpreted as mammal footprint (Allen, 1989, 1997). Above, a *ca* 15 m thick interval of medium tabular sandstones (F9), pervasively affected by palaeosoils, is in places intercalated by m-scale lenticular conglomerates (F11). Overlying, a prominent *ca* 6 m thick carbonate-rich interval (Figures 2 and 8f) shows alternations of bioclastic calci-mudstones (F3) and phytoherm boundstones of vertical stems (F4b), sporadically associated with bryoherm boundstones of mosses (F5). The succession ends with a finer version of tabular sandstones (F9) (Figure 8e) associated with rare lenticular sandstones and a *ca* 3 m thick muddy sandstones interval.

Coarse sandstones in the lowermost section 3 represent overbank deposits (Miall, 2014). Burrows and mammal footprints testify bioturbation by abundant fauna in a low-energy water-saturated environment. The facies association suggests clastic marsh environments, sporadically visited by large animals. Above, tabular and lenticular sandstones reflect overbank and channel deposits in an alluvial plain environment (Miall, 2014). Frequent rhizoliths point to abundant vegetation. The bioclastic calci-mudstones to wachestones and phytoherm boundstones reflect palustrine tufa sedimentation in a marshy, but less clastic environment, locally associated with ponds. Finally, the finer interval of tabular sandstones indicates a renewed alluvial plain environment.

Sequence analysis and significance
Field observations allow correlating two stratigraphic surfaces of sector 3 with the previously described sectors (Figure 2). Hence, the top of S2 is located at the top of palustrine tufa deposits in sector 3, while the top of S3 corresponds to the top of the succession (Figure 2). Sedimentation in sector 3 is indicative of a clastic-dominated fluvial to marsh environment, revealing that the palaeolake observed in the central portion of the depocentre did not extend up to this locality neither during S1 and S2, even if the uppermost part of S2 in sector 3 clearly displays deposits related to wetter environments. Here, the long-term aggradation of fluvial and palustrine deposits rather indicates that sediment supply was exceeding accommodation all along the activity of the depocentre, even during the transgressive periods observed in sectors 1 and 2.

4.1.5 | Sectors 4: North-western margin

Depositional environments
Sector 4 is located in the north-western part of the depocentre (Figure 1c). It represents a transitional zone between the internal and the external feijas that are connected through relatively narrow passes intersecting the Tabanit Ridge. No section was logged in sector 4, which mostly encompasses carbonate deposits (U9) forming a topographic step that connects the topographically higher internal feija with the lower external feija. U9 comprises several successive m-scale steps, oriented downstream towards the external feija (Figure 8g). The steps are formed by phytoherm boundstones of hanging stems (F4c) (Figure 8g,h) connected by planar beds consisting mostly of tabular microbial boundstones (F6a). U9 is onlapped by a *ca* 5 m thick mudstone succession (U10; Figure 8i) that includes clastic mudstones (F1) occasionally interbedded with dm-scale calci-mudstones intervals (F2) and rarely cm-scale to dm-scale lobate sandstones (F8). Finally, a *ca* 7 m thick sandstone succession referred to as U11 overlies both U10 and U9 (Figure 8i). U11 mostly includes tabular sandstones (F9).
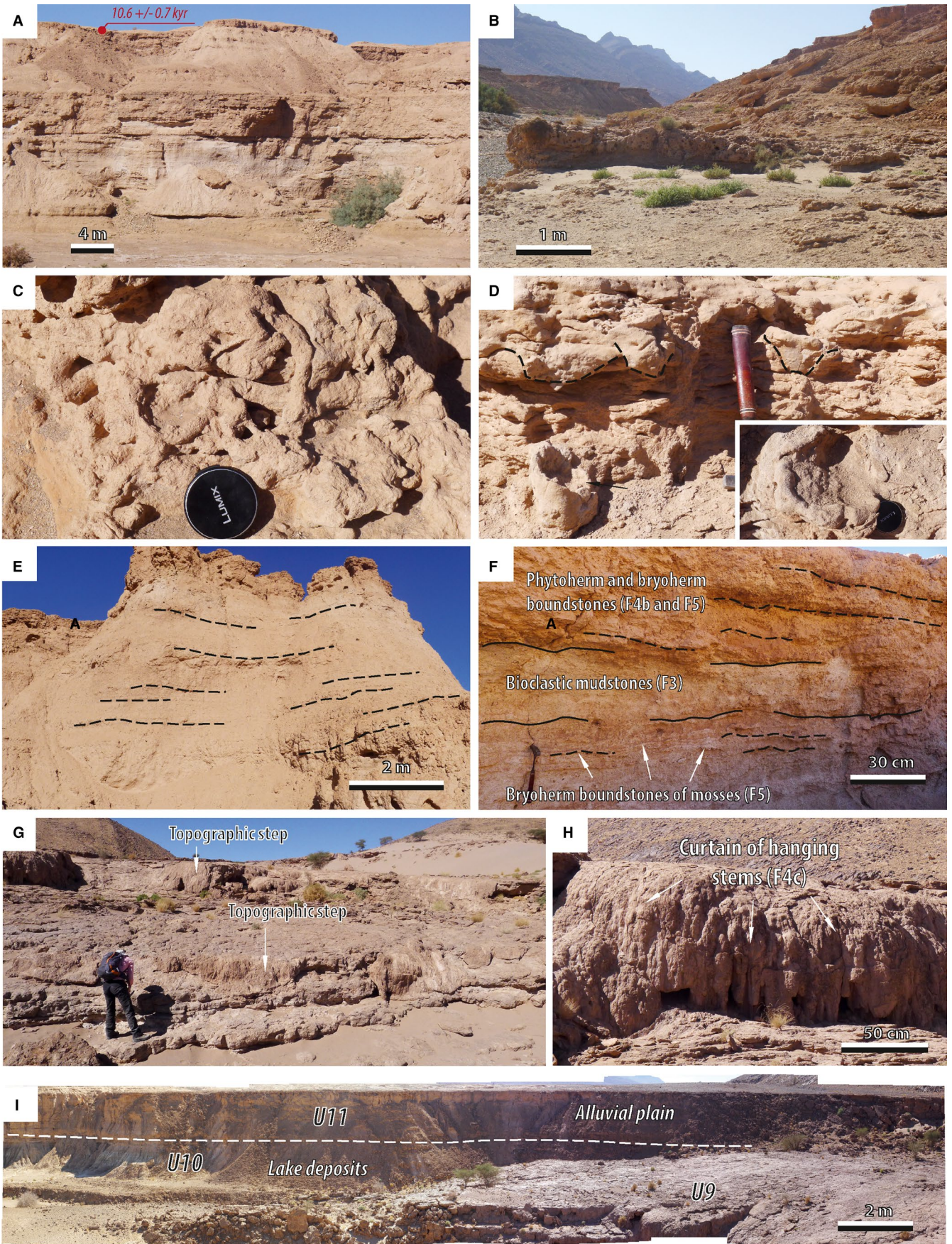
The m-scale steps composed of hanging stems in U9 represent successive cascades which form a large-scale topographic step interpreted as stepped fluvial tufa (cf. Arenas-Abad et al., 2010). Above, U10 reflects offshore lacustrine deposits in places interbedded by river mouth deposits. The overlying U11 is attributed to overbank deposits in an alluvial plain environment.

Sequence analysis and significance
Sedimentary units in sector 4 are directly correlated with units in sectors 1–3 and previously interpreted sequences can be delineated. Offshore lacustrine (U10) and floodplain (U11) deposits are laterally correlated with the offshore lacustrine (U3b) and alluvial plain (U4) deposits in the central portion of the depocentre, respectively. Hence, U10 and U11 coincide to S2 and S3, respectively. U9 is laterally associated with U1. The cascades in U9 corroborate a significant elevation change between the internal and the external feijas prior to sedimentation in the external feija, suggesting a preexisting depression in the external feija.

4.2 | Synthesis—Basin-scale transects and chronological constraints

Combining information from the four sectors described above, two basin-scale transects are reconstructed (Figure 9). They depict the basin-scale architecture of the depocentre. Three long-term sequences are identified (S1–S3), superimposed by shorter-term sequences in S1 and S2, best observed within the lacustrine deposits of the central sector. S1 and S2 were characterized by the existence of a palaeolake, hereafter referred to as palaeolake Tissint that repeatedly occupied a portion of the external feija in tune with repeated pulses of tufa dam aggradation. In the central portion, palaeolake Tissint was characterized by low-energy sedimentation of clastic or calci-mudstones and low-energy vegetated margins and shores. In front of rivers that entered the lake, sandy river mouth complexes developed. Estimated locations of palaeoshorelines suggest that palaeolake Tissint corresponded
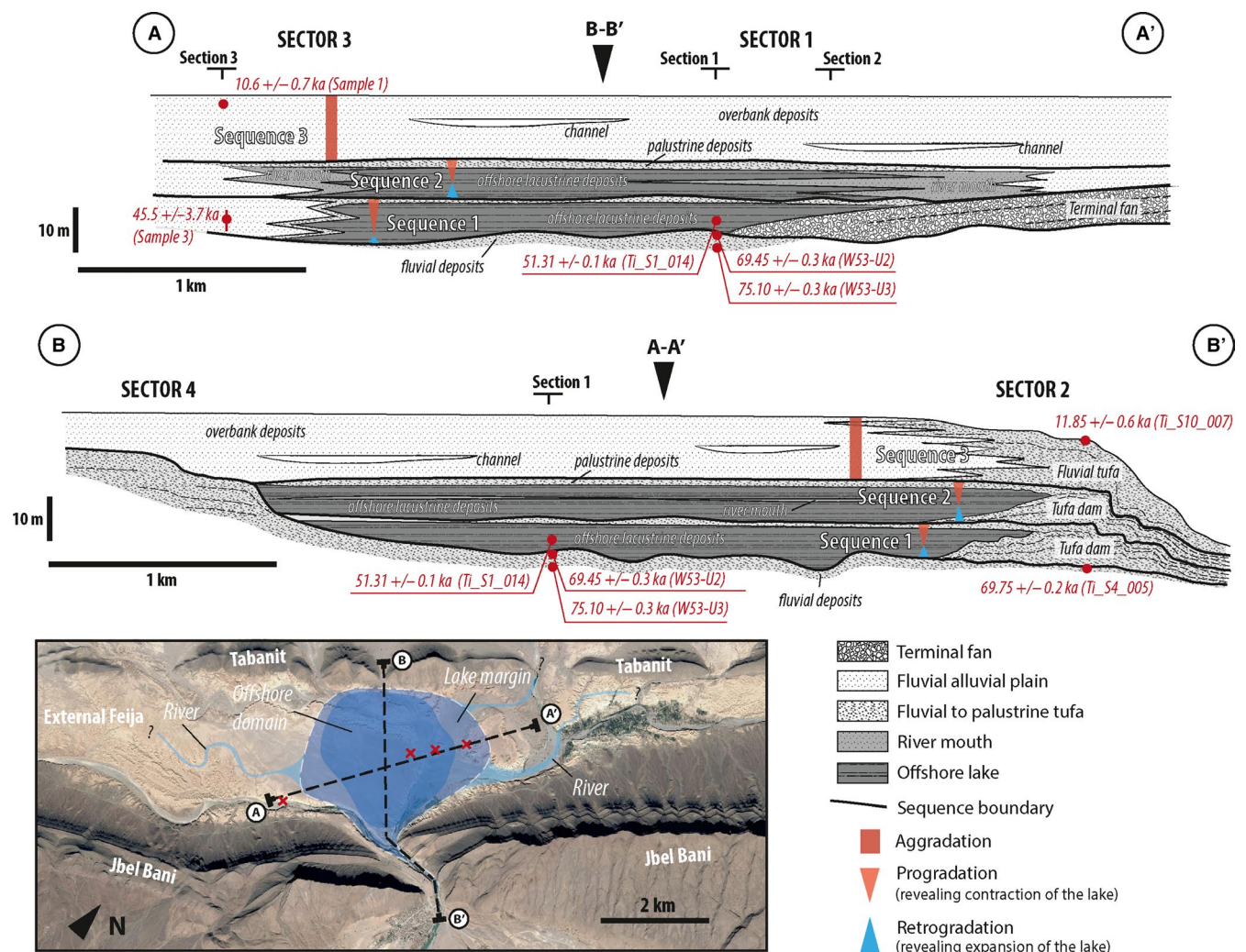
FIGURE 8 Sedimentary architectures and facies in sectors 3 and 4 (see locations Figure 1c). (a) Global view on section 3. (b) Coarse sandstones package within the lowermost part of section 3. (c) Burrows in coarse sandstones. (d) Mammal footprints in coarse sandstones. (e) Fine-grained tabular sandstones (F9) in the upper part of section 3. (f) Carbonate-rich interval including alternations of bioclastic mudstones (F3) and phytoherm boundstones of vertical stems (F4b) in places associated with bryoherm boundstones of mosses (F5). (g) Topographic steps constituting the surface of U9 in sector 4. (h) Close-up view on one of these topographic steps made of phytoherm boundstones of hanging stems. (i) Onlap of U10 and U11 onto U9

to an area of, at most, *ca* 10 km^2 (Figure 9) laterally associated with a vegetated fluvial floodplain. Finally, the top of S2 and S3 witnessed the disappearance of palaeolake Tissint. Subsequently, the Agadir-Tissint Feija was dominated by a coarser-grained sedimentation associated with an aggrading stepped fluvial tufa in the Tissint gorge (S3). At that time, the external feija was occupied by several tens of metres wide river channels laterally associated with overbank deposits.

Combining new radiometric dates (U/Th) with existing ages from literature (Thorp et al., 2002), eight ages are now available from different localities within the depocentre that constrain the temporal evolution of these sequences (Table 2; Figure 9). The age of the basal fluvial interval (U1) in the

central portion of the depocentre is estimated from three different U/Th dates between *ca* 75.10 ± 0.3 and 69.45 ± 0.1 kyr. Above, S1 is the first exposed lacustrine interval, associated laterally with a tufa dam in the gorge. Precise age of the onset of the transgression is not yet available, but the absence of significant alteration and/or soil development suggest that the interruption of deposition of the fluvial deposits was probably followed by a lacustrine transgression without long-term hiatus suggesting a flooding shortly after *ca* 69 kyr. A U/Th age from calci-mudstones in a stratigraphically higher interval within S1 (51.3 ± 0.1 kyr) is located just above the maximum flooding interval and is consistent with an earlier OSL age given by Thorp et al. (2002) in sector 3 indicating an age

FIGURE 9 Basin-scale synoptic transects of the external part of the Agadir-Tissint Feija. The three long-term sequences are represented. Note that shorter-term sequences are not represented. Reconstructed maximum palaeolimits of palaeolake Tissint during S1 and S2 are presented

of *ca* 45 ± 3.7 kyr in S1, although the precise location of this OSL analysis in our measured section is uncertain. In sector 2, two new U/Th ages bracket the succession. The lowermost part of the interval is dated at 69.75 ± 0.3 kyr; this remarkably matches with the age of the lowermost part of the succession in sector 1. Finally, another U/Th date (11.8 ± 0.6 kyr) at the top of S3 in sector 2 (Figure 9) is consistent within uncertainties with an OSL age of 10.6 ± 0.7 kyr provided by Thorp et al. (2002) found 0.4 cm below the top of S3. They characterize the age of the latest stage of sedimentation in the depocentre.

5 | INTERPRETATION AND DISCUSSION

5.1 | Palaeoenvironmental reconstructions

Analyses of architectures and facies distribution allowed the identification of different sedimentary systems in the Agadir-Tissint Feija. Their superimposition reveals the existence of several long-term and short-term sequences. These sequences express recurrent changes in water and sediment supply that necessarily derive from changes in palaeoenvironmental conditions. In the following, the long-term sequences in the depocentre are interpreted based on observations of the pulsed buildup of the tufa complex in the Tissint gorge. After discussing the mechanisms and palaeoenvironmental significance of tufa development, sedimentary systems that alternatively occupied the depocentre are described and framed in a comprehensive model of landscape evolution.

5.1.1 | Tufa dam evolution and accommodation space creation

Sedimentation in the Agadir-Tissint Feija during the late Quaternary required respective accommodation space. Correlations between lacustrine and aggrading alluvial plain deposits in the central portion of the depocentre and pulses of tufa constructions in the Tissint gorge testify that the Tissint gorge tufa repeatedly elevated the regional base level resulting in the successive creation of accommodation space.

Tufa formation is driven by CO_2 degassing in waters rich in both calcium and bicarbonate ions, leading to calcium carbonate deposition (e.g. Arenas-Abad et al., 2010; Fuller et al., 2011; Pentecost, 2005). Thus, drainage of uppermost Neoproterozoic to lowermost Cambrian carbonates in the catchment is an important prerequisite for tufa deposition in the Agadir-Tissint Feija. Moreover, gorge setting also favoured tufa construction. Hence, degassing of CO_2 is favoured in agitated waters with high velocity and turbulence which are influenced by flow direction and gradient of the substrate, with a direct positive correlation between water supply and tufa precipitation (Arenas et al., 2010, 2015; Auqué et al., 2014). Two particular settings

along a river increase water turbulence and velocity locally, facilitating the deposition of tufa dams; (a) knickpoints characterized by a sudden increase in slope along the river profile (Arenas-Abad et al., 2010; Glover & Robertson, 2003; Pena, Sancho, & Lozano, 2000) and (b) stream bed narrowing leading to more confined stream segments (Arenas et al., 2010). As a consequence, the morphology of the Tissint gorge makes it conducive to tufa deposition localized in this sector. Pulses of tufa buildup in the Tissint gorge must therefore be attributed to fluctuations in water supply through time. Wet conditions triggered tufa formation by providing sufficient water, while the physiography of the Tissint gorge favoured degassing of the water and thus tufa precipitation. Thus, the three identified pulses of tufa buildup are associated with humid periods. Two of them are supported by the coexistence of a pulse of kaolinite production in the catchment (Figure 2). During dry periods, less water reached the dam and the aggradation decreased or ceased completely. Finally, alternations between wet and dry periods during the late Quaternary are considered as the main mechanism behind cyclic tufa dam emplacement at the outlet of the system.

5.1.2 | Evolution of the palaeoenvironment

Facies and sequence analyses in the Agadir-Tissint Feija define four distinct sedimentary systems, each representing different sedimentary dynamics and consequently palaeolandscapes (Figure 10). These four sedimentary systems are referred to as (a) deep lacustrine, (b) shallow lacustrine, (c) marsh and (d) river. They reflect temporarily variable combinations of water and sediment supply in the area.

Deep lacustrine sedimentary system

This system is characterized by the existence of a large lake in the depocentre where clastic mudstones were deposited in a low-energy central domain. Along the shore, low-energy vegetated areas developed far from river systems, and several sandy river mouth complexes formed where river systems entered the lake. The deposition of clastic mudstones and the absence of calci-mudstones indicate continuous activity of rivers even if the confinement of the coarse-grained clastics input in river mouth complexes suggests a relatively moderate amount of sediment supply. The absence of calci-mudstones also testifies for a carbonate-undersaturated lake, suggesting overflow over the tufa dam in the gorge. Constant overflow led to a continuous renewal of water and limited calcium and carbonate ion concentration in the lake and thus localized carbonate precipitation along the shore and in the gorge where CO_2 degassing was favoured by turbulence. During the existence of a deep lacustrine sedimentary system, dam aggradation in the Tissint gorge directly controlled the lake level. This configuration is thought to be characteristic of
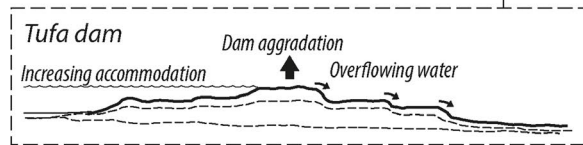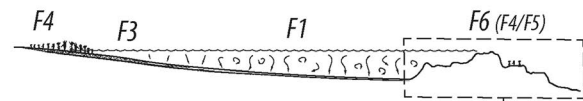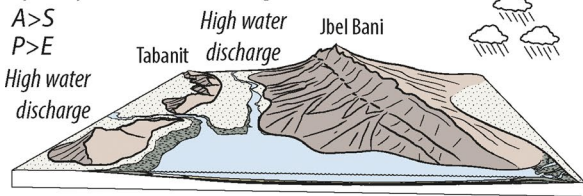
FIGURE 10 Sedimentary systems and resulting alternative palaeolandscapes that characterized the Agadir-Tissint Feija. Distribution of facies and the concomitant tufa dam configuration are presented for each palaeolandscape. Each palaeolandscape reflects a unique combination of precipitation amount and sediment supply in the depocentre. A = Accommodation; S = Sediment supply; P = Precipitation; E = Evaporation. The colour bar next to each case is used in Figure 11 to show the stratigraphic stacking of these systems during the late Quaternary

relative humid periods, when atmospheric precipitation exceeded evaporation and increased runoff delivered large amount of fine-grained sediments from the catchment.

Shallow lacustrine sedimentary system

This system is characterized by the existence of a reduced lake associated with calci-mudstone deposition in the central domain. The low-energy shore areas were vegetated. The deposition of calci-mudstones in the central portion of the basin necessitates carbonate supersaturation. The supersaturation could have been reached once the lake ceased overflowing and closed conditions promoted calcium ion concentration in the lake. During periods of shallow lake system, the tufa dam

was no more aggrading as the lake was no more overflowing. At the same time, the absence of both coarse-grained and fine-grained clastics in the lake sediments suggests either a reduced sediment production in the catchment area or a reduced transport capacity by rivers due to their very low activity. Shallow lacustrine systems are interpreted to represent intense, but short dry intervals superimposed on longer humid period.

Marsh sedimentary system

The marsh system is typified by a low-energy fluvial system in wetlands that occupied a large portion of the depocentre. Sedimentation was dominated by calcium carbonate

precipitation that formed basin-scale palustrine and fluvial tufa deposits. In this configuration, the tufa aggradation in the Tissint gorge ceased due to relatively drier conditions and insufficient water supply. At the same time, sediment supply was low as fine-grained sediment probably bypassed the depocentre while coarse-grained material was not transported up to the depocentre. Even the depocentre was characterized by wetlands; this configuration is considered as representative of a relative dry period in the overall catchment.

River sedimentary system

The river system consisted of a large alluvial plain that occupied the entire Agadir-Tissint Feija. Aggradation of alluvial plain sediments was linked to a pulsed buildup of fluvial tufa in the Tissint gorge, consistent with the notion of a contemporaneously increased water supply. Sediment supply was dominated by coarse-grained material, while fine-grained sediments were probably exported out of the depocentre. This suggests increased availability of coarse-grained material in the catchment under relatively humid conditions.

Synthesis

The vertical superposition of these four sedimentary systems (Figure 11) reflects the interplay between climatic factors and evolution of accommodation space in the depocentre. The three main sequences observed between *ca* 75 and *ca* 10 ka BP, and repeated pulse of tufa buildup in the Tissint gorge, are genetically attributable to three wetter periods. The two earlier ones were accompanied by a dominant production of fine-grained sediments in the catchment and reduced supply of coarse material in the depocentre. This configuration favoured the underfilled configuration that allowed the repeated development of palaeolake Tissint. Shorter-term sequences superimposed on these long-term changes reflect frequent lake-level fluctuations independent of tufa dam buildup. These fluctuations mark abrupt changes in the E/P ratio leading to alternations between an overflowing-deep lake and a closed-shallow lake. The third wet period was accompanied by the production of coarser material which led to an overfilled configuration and the establishment of the fluvial system. The possible mechanisms behind these climatic alternations and modification in sediment supply are discussed below.
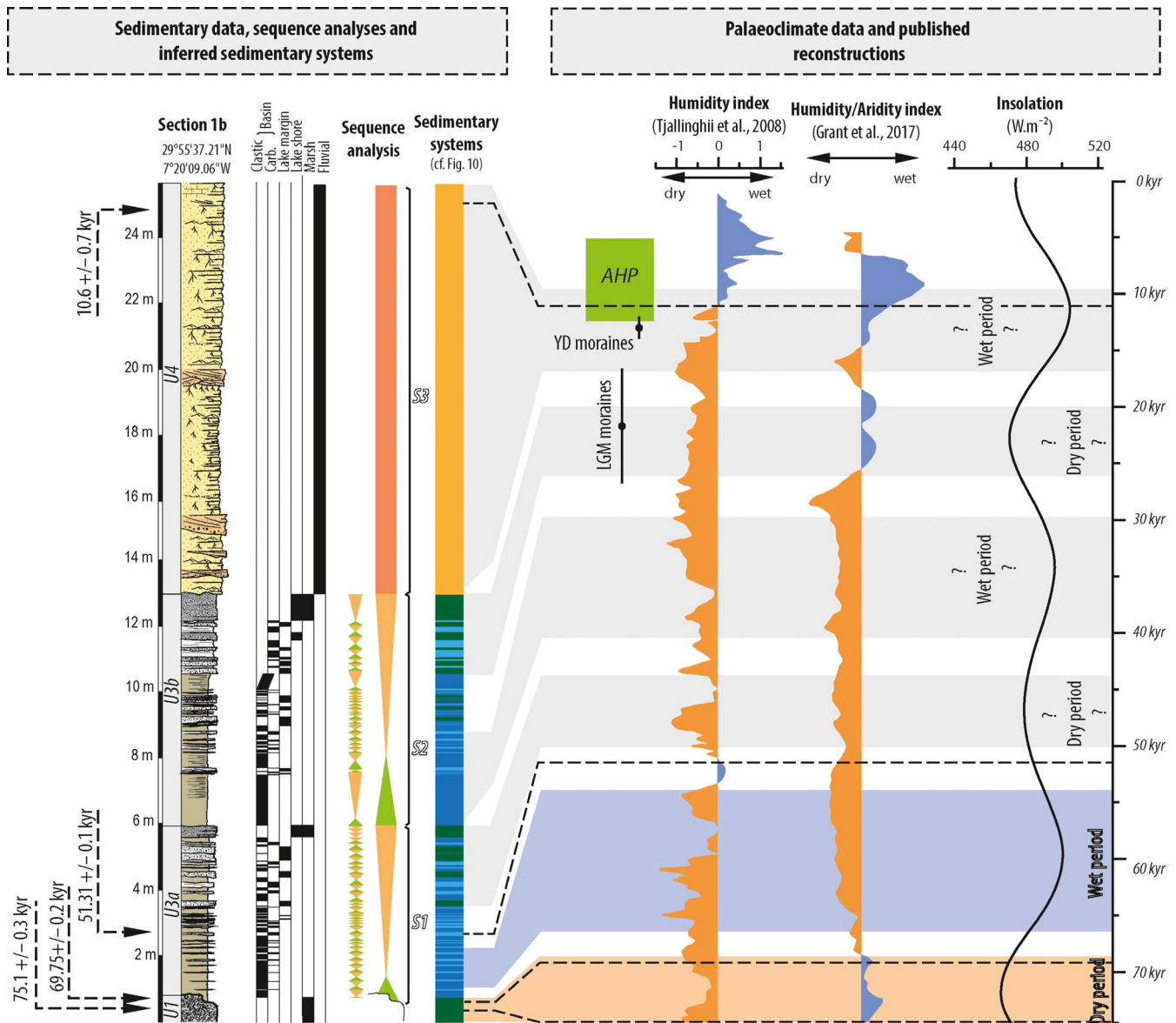
5.2 | Palaeoclimate perspectives

The climatic past of the northern Sahara margin has been investigated for more than 50 years. Indeed, pioneering studies (Rognon, 1980, 1987) of lacustrine/palustrine successions led to the identification of an important wet phase dated between 40 and 20 ka BP followed by a transition to the current aridity around 12–10 ka BP. More recently, palaeoclimate reconstructions based on marine sediment cores (Kuhlmann et al., 2004) identified a North Atlantic Oscillation (NAO) signal in palaeoclimate of northwest Africa (27°N) persisting over the last 9 kyr BP. Tierney et al. (2017) demonstrated that the last Green Sahara period extended to 31°N suggesting the monsoonal influence on the northern Sahara margin. Hence, different interpretations characterize a similar area and the sediment succession of the Agadir-Tissint Feija thus represents a valuable continental archive for discussing the contribution of these different potential influences on the northwest African palaeoclimate.

5.2.1 | Origin of wet–dry alternations: Implications for palaeoclimate in northwest Africa

Since the Late Miocene, African climate is known to be strongly influenced by insolation patterns mainly related to changes in precessional orbital parameters of the Earth (Larrasoana, Roberts, & Rohing, 2013). Cyclic changes in insolation have paced monsoon intensities and led to repeated humid episodes in Africa as well as important fluctuations of African lakes (e.g. Ashley, 2007; Nutz, Schuster, Boës, & Rubino, 2017; Schuster et al., 2005). In central Africa, recurrent humidification resulted in Green Sahara Periods (GSPs) associated with savannah expansion throughout most of the desert. More than 230 GSPs have occurred since the Miocene (Larrasoana et al., 2013). The penultimate GSP has been dated to between 81 and 77 ka (Larrasoana et al., 2013) and the last one to between 11 and 5 kyr BP (e.g. Bard, 2013; De Menocal et al., 2000). Between these two GSPs (i.e. *ca* 77–11 kyr), persistent drier conditions are suspected (Grant et al., 2017; Tjallingii et al., 2008).

The interval between *ca* 75 and 10 ka BP encompasses three precessional cycles with insolation minima around 74–68 ka BP, 50–44 ka and 26–20 ka and insolation maxima around 64–56 ka BP, 38–30 ka BP and 14–10 ka BP (Figure 11; Laskar et al., 2004). The relationship between insolation and palaeohydrology in the Agadir-Tissint Feija is suspected by available datings that indicate a relative dry period in the Agadir-Tissint Feija between 75 and 69 ka during a period concomitant to a minimum of insolation (74–68 ka BP). Additionally, the maximum flooding interval of S1 located between *ca* 69 ka and *ca* 51 ka fits with the age of an insolation maximum (64–56 ka BP). Thus, the timing of the well-dated wet–dry alternation associated with S1 in the Agadir-Tissint Feija matches broadly summer insolation changes, with a dry period corresponding to summer insolation minima and a humid period aligned with summer insolation maxima. Even though additional robust dates are needed to firmly correlate S2 and S3 to precession-paced wet–dry alternations, this finding strongly suggests orbital control on the environmental conditions in

FIGURE 11 Summary of sedimentary data, sequence analyses and inferred palaeoclimate evolution for the considered time interval (75–10 kyr BP). Long-term sequences are presented along section 1b, showing the stratigraphic evolution of sedimentary systems. Extrapolated timing of sequences S2 and S3 is represented based on the relation between S1 and the insolation curve (Laskar et al., 2004) suggesting that humid periods in the Agadir-Tissint Feija are correlated with high insolation periods. Regional humidity indexes (Grant et al., 2017; Tjallingii et al., 2008) reveal that humid periods recorded by S1 are not anticipated by these indexes. Timing of moraines development in the High Atlas Mountain (from Hughes et al., 2018) indicates a regional cooling probably related with the change in material production in the catchment and increased sediment supply in the depocentre during the LGM

the study area. At this point, considering precession-paced wet–dry cycles in the depocentre, the three pulses of dam buildup would have coincided with high insolation periods (*ca* 64–56 ka BP, *ca* 38–30 ka and *ca* 14–10 ka), separated by periods during which tufa buildup was prevented that are associated with low insolation (*ca* 74–68 ka BP, *ca* 50–44 ka and *ca* 26–20 ka). Superimposed, 33 and 26 shorter-term episodes of lake-level fall are recognized in S1 and S2 with a theoretical recurrence of 757 years in S1 and 992 years in S2, respectively. Given the uncertainties

of our chronology, this may match with the periodicity of *ca* 900 years identified by Kuhlmann et al. (2004) for the NAO. This NAO periodicity has been linked with north-west African climate (Trouet et al., 2009; Wassenburg et al., 2013); this mechanism—and the resulting long-term mean state of the NAO—could potentially be responsible for repeated drought episodes in the north-western Sahara margin. With regard to the palaeolake Tissint, further investigations are needed to robustly constrain the chronological scheme and the invoked North Atlantic forcing.

Finally, the sedimentary succession of the Agadir-Tissint Feija holds a sensitive continental palaeoclimate record for the north-western Sahara margin. First and foremost, it challenges the existence of a persistent drier period between 77 and 11 ka BP in northwest Africa as proposed in some previous studies (e.g. Grant et al., 2017; Tjallingii et al., 2008). Instead, the sedimentary succession of the Agadir-Tissint Feija clearly evidences that wetter conditions than today prevailed all along this time interval, perhaps enhanced during high insolation maxima. These new results tend to confirm that the monsoon influenced palaeoclimate in the north-western Sahara margin as proposed by Tierney et al. (2017) during the last GSP; moreover, they propose that monsoon also influenced climate during anterior high insolation periods that are not depicted as GSPs yet.

5.2.2 | Evolution of sediment supply: A signature of the last glacial maximum establishment

Sediment supply is controlled by sediment availability in the catchment and by river competence and capacity to transport sediments into the depocentre (summarized by Blum & Tornqvist, 2000). In the Agadir-Tissint Feija, during the deposition of S1 and S2, coarse material was either rare in the catchment or the transport capacity of the river was too low to significantly import grains larger than clay/silt. Construction of a tufa dam complex associated with a lacustrine transgression during both S1 and S2 suggest that rivers were active. This supports that the scarcity of coarse-grained detrital material in the depocentre at that time was probably due to the low availability of such material in the catchment rather than to the reduced transport capacity of the fluvial channels. Consequently, a lake developed in which fine-grained detrital material was deposited and the depocentre was underfilled. During the deposition of S3, the sedimentary record shows a sudden change in nature of sediment supply. Coarse-grained detrital material was transported and deposited to the depocentre. Greater sedimentation rate due to coarser sediments led to an overfilled configuration. Overfilling of the depocentre is thus interpreted as the expression of changes in the production and fragmentation, hence availability of coarse-grained detrital material in the catchment.

Assuming that precession cycles were the pacemaker for the long-term wet–dry cycles in the Agadir-Tissint Feija, the timing of the transition between these two sedimentation regimes broadly matches the timing of the last glacial maximum (LGM; Figure 11). Hughes, Fink, Rodés, Fenton, and Fujioka (2018) documented glaciers development and activity in some areas of the High Atlas Mountains during the last glacial cycle and the LGM. These authors revealed that the maximum advance of glaciers in the High Atlas Mountains reached 1,900–2,400 m in elevation while glaciers reached 2,200–2,600 m in elevation during the LGM. A last glacial advance is attributed to the Younger Dryas event. Comparable reliefs are absent in the Anti-Atlas range and with the maximum elevations around 1,900 to 2,000 m a.s.l., glaciers probably did not develop here. Still, significantly colder temperatures can be inferred. Colder temperatures would have led to more frequent freezing temperatures during winter, enhancing physical degradation by frost weathering (e.g. Matsuoka & Murton, 2008). Concomitantly, lower temperatures would have significantly reduced chemical weathering and the production of fine-grained detrital material. Thus, colder temperatures would have favoured fragmentation of rocks and generation of coarse-grained detrital material. Hence, the transition from mudstone-dominated to sandstone-dominated sediment observed in the Agadir-Tissint Feija is interpreted as being a response to the establishment of colder conditions probably associated with the LGM. This led to a transition from a chemically dominated weathering to a physically dominated degradation of rocks that modified the nature of supplied sediments.

6 | CONCLUSIONS

Measured sections, panoramas' interpretations and clay minerals analysis document deposits of the Agadir-Tissint Feija as a valid environmental archive, while radiometric datings identify it as a first well-constrained site in the continental north-western Africa for the last glacial cycle. A detailed analysis of sedimentary facies, facies distribution and basin-scale architectures permits determination of the sedimentary evolution through time of the Agadir-Tissint Feija between *ca* 75 and 10 kyr. Two basin-scale transects summarize the basin-scale architecture of the depocentre and four reconstructed depositional systems illustrate the successive palaeoenvironments.

Three distinct depositional sequences referred to as S1, S2 and S3 were deposited between *ca* 75 and 10 ka. They originated from three pulsed buildups of a carbonate tufa complex at the outlet of the depocentre that successively provided accommodation space within the feija. S1 and S2 both display the emplacement of a perennial palaeo-lake intercalated by periods characterized by carbonate-rich fluvial to marsh depositional systems. In S1 and S2, the palaeolake includes 33 and 26 shorter-term lake-level drops, respectively, revealing repeated shorter-term fluctuations in E/P ratio. Above, S3 consists of a fluvial interval made of alluvial plain deposits linked to the sudden increase of supply in coarse-grained detrital sediments that overfilled the depocentre and prevented a third reoccurrence of the palaeolake. S1 is correlated with a precession cycle, while S2 and S3 are suspected to be correlated with precession cycles even if additional dates are necessary to

confirm it. Nevertheless, S1 indicates that monsoonal influence reached N30° in northwest Africa. On the other hand, shorter-term fluctuations are suspected to be tuned to the NAO, suggesting an influence of the North Atlantic system on northern Sahara climate even if further investigations are needed to confirm this latter point. Finally, the sudden increase in coarse granular sediments is attributed to an enhanced frost weathering in the catchment area due to colder temperatures associated with the last glacial cycle and the LGM.

The repeated occurrences of relative long-term lacustrine conditions in the north-western Sahara margin during the last glacial reported for the first time, challenge persistent aridity in this region proposed in previous studies (e.g. Grant et al., 2017; Tjallingii et al., 2008). Also, with the sedimentary evolution of the "Agadir-Tissint Feija" considered as representative to other "feijas" along the southern flank of the Anti-Atlas in southern Morocco, these systems will constitute valuable new archives for Late Quaternary palaeoclimate in northwest Africa.

ACKNOWLEDGEMENTS

CONFLICT OF INTEREST

The authors have no conflict of interest to declare.

ORCID

Alexis Nutz https://orcid.org/0000-0002-8224-5639

REFERENCES

Allen, J. R. L. (1989). Short paper: Fossil vertebrate tracks and indenter mechanics. *Journal of the Geological Society, London*, *46*, 600–602. https://doi.org/10.1144/gsjgs.146.4.0600

Allen, J. R. L. (1997). Subfossil mammalian tracks (Flandrian) in the Severn Estuary, S.W. Britain: Mechanics of formation, preservation and distribution. *Philosophical Transactions of the Royal Society of London Series B*, *352*, 481–518. https://doi.org/10.1098/rstb.1997.0035

Alvaro, J. J., Benziane, F., Thomas, B., & Walsh, G. J. (2014). Neoproterozoic-Cambrian stratigraphic framework of the anti-Atlas and Ouzellagh promontory (High Atlas), Morocco. *Journal of African Earth Sciences*, *98*, 19–33. https://doi.org/10.1016/j.jafrearsci.2014.04.026

Andres, W. (1977). Studien zur jungquartären Reliefentwicklung des sudwestlichen Anti-Atlas und seines saharischen Vorlandes (Marokko), Mainzer Geographischen Studien Ht. 9, Mainz.

Arenas, C., Auqué, L., Oscar, C., Sancho, C., Lozano, M. V., Vazquez-Urbez, M., & Pardo, G. (2015). Current tufa sedimentation in a high discharge river: A comparison with other synchronous tufa records in the Iberian Range (Spain). *Sedimentary Geology*, *325*, 132–157. https://doi.org/10.1016/j.sedgeo.2015.05.007

Arenas, C., Osacar, C., Sancho, C., Vazquer-Urbez, M., Auqué, L., & Pardo, G. (2010). Seasonal record from recent fluvial Tufa deposits (Monasterio de Piedra, NE Spain): Sedimentological and stable isotope data. In M. Pedley, & M. Rogerson (Eds.), *Tufas and speleothems: Unravelling the microbial physical controls. Geological Society, London, Special Publications*, *336*, 119–142.

Arenas-Abad, C., Vazquez-Urbez, M., Pardo-Tirapu, G., & Sancho-Marcéen, C. (2010). Fluvial and associated carbonate deposits. In A. M. Alonzo-Zarza & L. H. Tanner (Eds.), *Carbonates in continental settings: Facies, environments and processes. Developments in Sedimentology*, *61*, 133–175. https://doi.org/10.1016/S0070-4571(09)06103-2

Arribas, M. E., Bustillo, A., & Tsige, M. (2003). Lacustrine chalky carbonates: Origin, physical properties and diagenesis (Palaeogene of the Madrid Basin, Spain). *Sedimetnary Geology*, *166*, 335–351.

Ashley, G. M. (2007). Orbital rhythms, monsoons and playa lake response, Olduvai Basin, equatorial East Africa (*ca.* 1.85-1.74). *Geology*, *35*, 1091–1094. https://doi.org/10.1130/G24163A.1

Auqué, L., Arenas, C., Osacar, C., Pardo, G., Sancho, C., & Vazquez-Urbez, M. (2014). Current tufa sedimentation in a changing-slope valley: The River Anamaza (Iberian Range, NE Spain). *Sedimentary Geology*, *303*, 26–48. https://doi.org/10.1016/j.sedgeo.2014.01.008

Bard, E. (2013). Out of the African humid period. *Science*, *342*, 808–809. https://doi.org/10.1126/science.1246519

Blum, M. D., & Tornqvist, T. E. (2000). Fluvial responses to climate and sea-level change: A review and look forward. *Sedimentology*, *47*, 2–48. https://doi.org/10.1046/j.1365-3091.2000.00008.x

Burkhard, M., Caritg, S., Helg, U., Robert-Charrue, Ch, & Soulaimani, A. (2006). Tectonics of the anti-atlas of Morocco. *Compte Rendus Geoscience*, *338*, 11–24. https://doi.org/10.1016/j.crte.2005.11.012

Bustillo, M. A., Arribas, M. E., & Bustillo, M. (2002). Dolomitization and silicification in low-energy lacustrine carbonates (Paleogene, Madrid Basin, Spain). *Sedimentary Geology*, *151*, 107–126. https://doi.org/10.1016/S0037-0738(01)00234-2

Catuneanu, O., Abreu, V., Bhattacharya, J. P., Blum, M. D., Dalrymple, R. W., Eriksson, P. G., … Winker, C. (2009). Towards the standardization of sequence stratigraphy. *Earth-Science Reviews*, *92*, 1–33. https://doi.org/10.1016/j.earscirev.2008.10.003

Chamley, H. (1989). *Clay sedimentology*. Heidelberg, Germany: Springer, 623 pp. https://doi.org/10.1007/978-3-642-85916-8

Cheng, H., Edwards, R. L., Shen, C. C., Polyak, V. J., Asmerom, Y., Woodhead, J., … AlexanderJr, E. C. (2013). Improvements in ^{230}Th datings, ^{230}TH and ^{234}U half-life values, and U-Th isotopic measurements by multi-collector inductively coupled plasma mass spectrometry. *Earth and Planetary Science Letters*, *371-372*, 82–91. https://doi.org/10.1016/j.epsl.2013.04.006

De Menocal, P., Ortiz, J., Guilderson, T., Adkins, J., Sarnthein, M., Baker, L., & Yarusinsky, M. (2000). Abrupt onset and termination of the African humid period: Rapid climate responses to gradual insolation forcing. *Quaternary Science Reviews*, *19*, 347–361. https://doi.org/10.1016/S0277-3791(99)00081-5

Della Porta, G. (2015). Carbonate build-ups in lacustrine, hydrothermal and fluvial settings: Comparing depositional geometry, fabric types and geochemical signature. In D. W. J. Bosence, K. A. Gibbons, D. P. Le Heron, W. A. Morgan, T. Pritchard, & B. A. Vining (Eds.),

Microbial carbonates in space and time: Implications for global exploration and production. Geological Society, London, Special Publications, *418*, 17–68.

Della Porta, G., Capezzuoli, E., & De Bernardo, A. (2017). Facies character and depositional architecture of hydrothermal travertine slope aprons (Pleistocene, Acquasanta Terme, Central Italy). *Marine and Petroleum Geology*, *87*, 171–187. https://doi.org/10.1016/j.marpetgeo.2017.03.014

Dietrich, P., Ghienne, J-F., Lajeunesse, P., Normandeau, A., Deschamps, R., & Razin, Ph. (2018). Deglacial sequences and glacio-isostatic adjustment: Quaternary compared to Ordovician glaciations. In D. P. Le Heron, K. A. Hogan, E. R. Phillips, M. Huuse, M. E. Busfield, & A. G. C. Graham (Eds.), *Glaciated Margins: The sedimentary and geophysical archive. Geological Society, London, Special Publications*, *475*. https://doi.org/10.1144/SP475.9

Dijon, R. (1976). Reconnaissance hydrologique et ressources en eau du bassin des Oueds Seyad-Ouarg Noun, Maroc sud-occidental, Notes Mem. Serv. Géol. Maroc., Rabat, N°.197.

Edwards, R. L., Chen, J. H., Ku, T. L., & Wasserburg, G. J. (1987). Precise timing of the last interglacial period from mass spectrometric determination of thorium-230 in corals. *Science*, *236*, 1547–1553. https://doi.org/10.1126/science.236.4808.1547

Fang, X., Wang, J., Zhang, W., Zan, J., Song, C., Yan, M., … Lu, Y. (2016). Tectonosedimentary evolution model of an intracontinental flexural (foreland) basin for paleoclimatic research. *Global and Planetary Change*, *145*, 78–97. https://doi.org/10.1016/j.gloplacha.2016.08.015

Ford, T. D., & Pedley, H. M. (1996). A review of tufa and travertine deposits of the world. *Earth-Science Reviews*, *41*, 117–175. https://doi.org/10.1016/S0012-8252(96)00030-X

Fuller, B. M., Sklar, L. S., Compson, Z. G., Adams, K. J., Marks, J. C., & Wilcox, A. C. (2011). Ecogeomorphic feedbacks in regrowth of travertine step-pool morphology after dam decommissioning, Fossil Creek, Arizona. *Geomorphology*, *126*, 314–332. https://doi.org/10.1016/j.geomorph.2010.05.010

Gasquet, D., Ennih, N., Liégeois, J. P., Soulaimani, A., & Michard, A. (2008). The Pan-African belt. In A. Michard, A. Chalouan, O. Saddiqi, & de Lamotte D. (Eds.), *Continental evolution: The geology of Morocco, structure, stratigraphy, and tectonics of the African-Atlantic-mediterranean triple junction. Lecture Notes in Earth Sciences*, *116*,33–64.

Ghienne, J.-F., Le Heron, D., Moreau, J., Denis, M., & Deynoux, M. (2007). The Late Ordovician glacial sedimentary system of the North Gondwana platform. In M. Hambrey, P. Christoffersen, N. Glasser, P. Janssen, B. Hubbard, & M. Siegert (Eds.), *Glacial sedimentary processes and products*. Special Publication no. 39, International Association of Sedimentologist (pp. 295–319). Oxford, UK: Blackwell.

Glover, C., & Robertson, A. H. F. (2003). Origin of tufa (cool-water carbonate) and related terraces in the Antalya area, SW Turkey. *Geological Journal*, *38*, 329–358. https://doi.org/10.1002/(ISSN)1099-1034

Godard, V., Bourlès, D. L., Spinabella, F., Burbank, D. W., Bookhagen, B., Burch Fisher, G., … Léanni, L. (2014). Dominance of tectonic over climate in Himalayan denudation. *Geology*, *42*, 243–246. https://doi.org/10.1130/G35342.1

Google earth Pro. (2016). Tissint, Morocco. Retrieved from http://www.earth.google.com

Gradziński, M. (2010). Factors controlling growth of modern tufa: Results of a field experiment. In H. M. Pedley & M. Rogerson (Eds.), *Tufas and Speleothemes – Unravelling the microbial and physical controls. Geological Society, London, Special Publications*, *336*(1), 143–191.

Grant, K. M., Rohling, E. J., Westerhold, T., Zabel, M., Heslop, D., Konijnendjik, T., & Lourens, L. (2017). A 3 million year index for North African humidity/aridity and the implication of potential pan-African Humid periods. *Quaternary Science Reviews*, *171*, 100–118. https://doi.org/10.1016/j.quascirev.2017.07.005

Hughes, Ph.D, Fink, D., Rodés, A., Fenton, C. R., & Fujioka, T. (2018). Timing of Pleistocene glaciations in the High Atlas, Morocco: New [10]Be and [36]Cl exposure ages. *Quaternary Science Reviews*, *180*, 193–213. https://doi.org/10.1016/j.quascirev.2017.11.015

Kuhlmann, H., Meggers, H., Freudenthal, T., & Wefer, G. (2004). The transition of the monsoonal and the N Atlantic climate system off NW Africa during the Holocene. *Geophysical Research Letters*, *31*, L22204.

Larrasoana, J. C., Roberts, A. P., & Rohing, E. J. (2013). Dynamics of green sahara periods and their role in hominin evolution. *PLoS ONE*, *8*, e76514. https://doi.org/10.1371/journal.pone.0076514

Laskar, J., Robutel, P., Joutel, F., Gastineau, M., Correia, A. C. M., & Levrard, B. (2004). A long term numerical solution for the insolation quantites of the Earth. *Astronomy & Astrophysics*, *428*, 261–285. https://doi.org/10.1051/0004-6361:20041335

Loi, A., Ghienne, J-F., Dabard, M.P., Paris, F., Botquelen, A., Christ, N., … Destombes, J. (2010). The Late Ordovician glacio-eustatic record from a high-latitude storm-dominated shelf succession: The Bou Ingarf section (Anti-Atlas, Southern Morocco). *Palaeogeography, Palaeoclimatology, Palaeoecology*, *296*, 332–358. https://doi.org/10.1016/j.palaeo.2010.01.018

Maloof, A. C., Ramezani, J., Bowring, S. A., Fike, D. A., Porter, S. M., & Mazouad, M. (2010). Constraints on early Cambrian carbon cycling from the duration of the Nemakit-Daldynian-Tommotian boundary 13C shift, Morocco. *Geology*, *38*, 623–626. https://doi.org/10.1130/G30726.1

Mather, A. E., Stokes, M., & Whitfield, E. (2017). Rivers terraces and alluvial fans: The case for an integrated Quaternary fluvial archive. *Quaternary Science Reviews*, *166*, 74–90. https://doi.org/10.1016/j.quascirev.2016.09.022

Matsuoka, N., & Murton, J. (2008). Frost weathering: Recent advances and future directions. *Permafrost and Periglacial Processes*, *19*, 195–210. https://doi.org/10.1002/(ISSN)1099-1530

Miall, A. D. (2014). *Fluvial depositional systems*. Springer. https://doi.org/10.1007/978-3-319-00666-6

Michard, A. (1976). Eléments de géologie marocaine. *Notes et Mémoires du Service Géologique*, *252*, 408.

Michard, A., Hoepffner, C., Soulaimani, A., & Baidder, L. (2008). The variscan belt. In A. Michard, O. Saddiqi, A. Chalouan, & de Frizon Lamotte D. (Eds.), *Continental evolution: The geology of Morocco*, Lecture Notes in Earth Sciences, vol. 126 (pp. 65–132). Berlin, Heidelberg, Germany: Springer. https://doi.org/10.1007/978-3-540-77076-3

Nutz, A., Ghienne, J.-F., Schuster, M., Dietrich, P., Roquin, C., Hay, M. B., … Cousineau, P. A. (2015). Forced regressive deposits of a deglaciation sequence: Example from the Late Quaternary succession in the Lake Saint-Jean basin (Québec, Canada). *Sedimentology*, *62*, 1573–1610. https://doi.org/10.1111/sed.12196

Nutz, A., Ghienne, J.-F., & Storch, P. (2013). Circular, cryogenic structures from the Hirnantian deglaciation sequence (Anti-Atlas, Morocco). *Journal of Sedimentary Research*, *83*, 115–131. https://doi.org/10.2110/JSR.2013.11

Nutz, A., Schuster, M., Boës, X., & Rubino, J.-L. (2017). Orbitally-driven evolution of Lake Turkana (Turkana Depression, Kenya, EARS) between 1.95 and 1.72 Ma: A sequence stratigraphy perspective. *Journal of African Earth Sciences*, *125*, 1–14.

Pedley, H. M. (1990). Classification and environmental models of cool freshwater tufas. *Sedimentary Geology*, *68*, 143–154. https://doi.org/10.1016/0037-0738(90)90124-C

Pena, J. L., Sancho, C., & Lozano, M. V. (2000). Climatic and tectonic significance of Pleistocene and Holocene tufa deposits in the Mijares River canyon, eastern Iberian range, Northeastern Spain. *Earth Surface Processes and Landforms*, *25*, 1403–1417. https://doi.org/10.1002/1096-9837(200012)25:13<1403::AID-ESP147>3.0.CO;2-N

Pentecost, A. (2005). *Travertine*. Berlin, Germany: Springer, 448 pp.

Potter, P. E., Maynard, J. B., & Pryor, W. A. (1980). *Sedimentology of shale*. New York, NY: Springer Verlag. https://doi.org/10.1007/978-1-4612-9981-3

Rognon, P. (1980). Une extension des déserts (Sahara et Moyen-Orient) au cours du Tardiglaciaire (18 000-10 000 ans BP). *Revue de Géologie dynamique et de Géographie Physique*, *22*, 313–328.

Rognon, P. (1987). Aridification and abrupt climatic events on the Saharan northern and southern margins, 20,000 y BP to present. In W. H. Berger & L. D. Labeyrie (Eds.), *Abrupt climatic change* (pp. 209–220). Dordrecht, The Netherlands: Springer. https://doi.org/10.1007/978-94-009-3993-6

Rott, E., Hotzy, R., Cantonati, M., & Sanders, D. (2012). Calcification types of Oocardium stratum Nägeli and microhabitat conditions in springs of the Alps. *Freshwater Science*, *31*(2), 610–624. https://doi.org/10.1899/11.084.1

Schomacker, E. R., Kjemperud, A. V., Nystuen, J. P., & Jahren, J. S. (2010). Recognition and significance of sharp-based mouth-bar deposits in the Eocene Green River Formation, Uinta Basin, Utah. *Sedimentology*, *57*, 1069–1087. https://doi.org/10.1111/j.1365-3091.2009.01136.x

Schuster, M., Roquin, C., Duringer, P., Brunet, M., Caugy, M., Fontugne, M., … Ghienne, J.-F. (2005). Holocene Lake Mega-Chad palaeoshorelines from space. *Quaternary Science Reviews*, *24*, 1821–1827. https://doi.org/10.1016/j.quascirev.2005.02.001

Terrizzano, C. M., Garcia Morabito, E., Christl, M., Likerman, J., Tobal, J., Yamin, M., & Zech, R. (2017). Climatic and tectonic forcing on alluvial fans in the Southern Central Andes. *Quaternary Science Reviews*, *172*, 131–141. https://doi.org/10.1016/j.quascirev.2017.08.002

Thomas, R. J., Fekkak, A., Ennih, N., Errami, E., Loughlin, S. C., Gresse, P. G., … Liégeois, J.-P. (2004). A new lithostratigraphic framework for the Anti-Atlas Orogen, Morocco. *Journal of African Earth Sciences*, *39*, 217–226. https://doi.org/10.1016/j.jafrearsci.2004.07.046

Thorp, M., Glanville, P., Stokes, S., & Bailey, R. (2002). Preliminary optical and radiocarbon age determinations for Upper Pleistocene alluvial sediments in the southern Anti Atlas Mountains, Morocco. *Compte Rendus Geoscience*, *334*, 903–908. https://doi.org/10.1016/S1631-0713(02)01831-X

Tierney, J. E., Pausata, F. S. R., & deMenocal, P. B. (2017). Rainfall regimes of the Green Sahara. *Science Advances*, *3*, e1601503. https://doi.org/10.1126/sciadv.1601503

Tjallingii, R., Claussen, M., Stuut, J.-B. W., Fohlmeister, J., Jahn, A., Bickert, T., … Rohl, U. (2008). Coherent high- and low-latitude control of the northwest African hydrological balance. *Nature Geosciences*, *1*, 670–675. https://doi.org/10.1038/ngeo289

Trouet, V., Esper, J., Graham, N. E., Baker, A., Scourse, J. D., & Frank, D. C. (2009). Persistent positive North Atlantic Oscillation mode dominated the Medieval climate anomaly. *Science*, *324*, 78–80. https://doi.org/10.1126/science.1166349

Van Dijk, M., Postma, G., & Kleinhans, M. G. (2009). Autocyclic behaviour of fan deltas: An analogue experimental study. *Sedimentology*, *56*, 1569–1589. https://doi.org/10.1111/j.1365-3091.2008.01047.x

Vazquez-Urbez, M., Arenas, C., & Pardo, G. (2012). A sedimentary facies model for stepped, fluvial tufa systems in the Iberian Range (Spain): The Quaternary Piedra and Mesa valleys. *Sedimentology*, *59*, 502–526. https://doi.org/10.1111/j.1365-3091.2011.01262.x

Wassenburg, J. A., Immenhauser, A., Richter, D. K., Niedermayr, A., Riechelmann, S., Fietzke, J., … Esper, J. (2013). Moroccan speleothem and tree ring records suggest a variable positive state of the North Atlantic Oscillation during the Medieval warm period. *Earth and Planetary Science Letters*, *375*, 291–302. https://doi.org/10.1016/j.epsl.2013.05.048

Weisrock, A. L. (2003). About the dating of Upper-Pleistocene fluvial deposits in the arid zone of Morocco: Comparative data of radiocarbon, optic stimulation luminescence and uranium/thorium methods. *Compte Rendus Geoscience*, *335*, 277–278. https://doi.org/10.1016/S1631-0713(03)00048-8

Wright, V. P. (1992). A revised classification of limestones. *Sedimentary Geology*, *76*(3–4), 177–185. https://doi.org/10.1016/0037-0738(92)90082-3

Zielhofer, Ch, Fletcher, W. J., Mischke, S., De Batist, M., Campbell, J. F. E., Joannin, S., … Mikdad, A. (2017). Atlantic forcing of Western Mediterranean winter rain minima during the last 12,000 years. *Quaternary Science Reviews*, *157*, 29–51. https://doi.org/10.1016/j.quascirev.2016.11.037